Atmos. Chem. Phys., 11, 12475–12498, 2011
www.atmos-chem-phys.net/11/12475/2011/
doi:10.5194/acp-11-12475-2011

Atmospheric Chemistry and Physics

Determination of tropospheric vertical columns of NO_2 and aerosol optical properties in a rural setting using MAX-DOAS

J. D. Halla[1], T. Wagner[2], S. Beirle[2], J. R. Brook[3], K. L. Hayden[3], J. M. O'Brien[3], A. Ng[4], D. Majonis[1,*], M. O. Wenig[5], and R. McLaren[1]

[1]Centre for Atmospheric Chemistry, York University, Toronto, ON, Canada
[2]Satellite Group, Max Planck Institute for Chemistry, Mainz, Germany
[3]Air Quality Research Division, Environment Canada, Toronto, ON, Canada
[4]Ontario Ministry of the Environment, Toronto, ON, Canada
[5]School of Energy and Environment, City U, Hong Kong, China
[*]now at: Department of Chemistry, University of Toronto, Toronto, ON, Canada

Received: 15 March 2011 – Published in Atmos. Chem. Phys. Discuss.: 27 April 2011
Revised: 25 November 2011 – Accepted: 1 December 2011 – Published: 13 December 2011

Abstract. Multi-AXis Differential Optical Absorption Spectroscopy (MAX-DOAS) measurements were performed in a rural location of southwestern Ontario during the Border Air Quality and Meteorology Study. Slant column densities (SCDs) of NO_2 and O_4 were determined using the standard DOAS technique. Using a radiative transfer model and the O_4 SCDs, aerosol optical depths were determined for clear sky conditions and compared to OMI, MODIS, AERONET, and local $PM_{2.5}$ measurements. This aerosol information was input to a radiative transfer model to calculate NO_2 air mass factors, which were fit to the measured NO_2 SCDs to determine tropospheric vertical column densities (VCDs) of NO_2. The method of determining NO_2 VCDs in this way was validated for the first time by comparison to composite VCDs derived from aircraft and ground-based measurements of NO_2. The new VCDs were compared to VCDs of NO_2 determined via retrievals from the satellite instruments SCIAMACHY and OMI, for overlapping time periods. The satellite-derived VCDs were higher, with a mean bias of $+0.5$–0.9×10^{15} molec cm^{-2}. This last finding is different from previous studies whereby MAX-DOAS geometric VCDs were higher than satellite determinations, albeit for urban areas with higher VCDs. An effective boundary layer height, BLH_{eff}, is defined as the ratio of the tropospheric VCD and the ground level concentration of NO_2. Variations of BLH_{eff} can be linked to time of day, source region, stability of the atmosphere, and the presence or absence of elevated NO_x sources. In particular, a case study is shown where a high VCD and BLH_{eff} were observed when an elevated industrial plume of NO_x and SO_2 was fumigated to the surface as a lake breeze impacted the measurement site. High BLH_{eff} values ($\sim$1.9 km) were observed during a regional smog event when high winds from the SW and high convection promoted mixing throughout the boundary layer. During this event, the regional line flux of NO_2 through the region was estimated to be greater than 112 kg NO_2 km^{-1} h^{-1}.

Correspondence to: R. McLaren
(rmclaren@yorku.ca)

1 Introduction

The role of nitrogen oxides in the atmosphere is paramount in atmospheric chemistry due to the deleterious effects they have on the atmosphere and biosphere. Recent estimates of global emissions of NO_x ($NO_2 + NO$) to the atmosphere fall in the range of 43–46 Tg N yr^{-1} (Jacob, 1999; Martin et al., 2003, 2006) using both bottom up and top down approaches. Approximately 74% of these emissions are attributable to anthropogenic and biomass burning sources. In the troposphere, the main source of ground state oxygen atoms, $O(^3P)$, is the photolysis of NO_2, Reaction (R1), which subsequently reacts with molecular oxygen to form ozone, Reaction (R2), collectively the two most important reactions in the photochemical formation of ground level ozone (Finlayson-Pitts and Pitts, 1999).

$$NO_2 + h\nu(\lambda < 420\,\text{nm}) \rightarrow O(^3P) + NO \quad \text{(R1)}$$

$$O(^3P) + O_2 + M \rightarrow O_3 + M \quad \text{(R2)}$$

The main losses of NO_2 in the atmosphere are through the photochemical formation of HNO_3 during the daytime,

Published by Copernicus Publications on behalf of the European Geosciences Union.

followed by dry and wet deposition, and through the formation of the nitrate radical, NO_3, and dinitrogen pentoxide, N_2O_5, at night. Hydrolysis of N_2O_5 on aerosols and cloud droplets to form HNO_3 and particle nitrate (McLaren et al., 2004) is thought to be the main removal mechanism for NO_x in the atmosphere at night (Dentener and Crutzen, 1993). Heterogeneous reaction of NO_2 on surfaces coated with water to form HONO at night is also known to be an important reaction in the atmosphere, as photolysis of HONO is known to be a major source of OH in the morning boundary layer (Platt and Perner, 1980), and has been estimated to contribute up to 30 % of the total OH production integrated over 24 h in polluted environments (Alicke et al., 2003). For these and other reasons, measurement of NO_2 in the troposphere is important.

Concentrations of NO_2 at ground level can be measured via chemiluminescence instruments and through active DOAS (Platt and Stutz, 2008). Multi-AXis Differential Optical Absorption Spectroscopy (MAX-DOAS) can also be used for the measurement of certain molecules such as NO_2 and O_4 through the application of the DOAS technique to spectra of sky scattered sunlight to identify and quantify column abundances of trace gases that have narrow band absorption structures in the near UV and Vis wavelength range (Hönninger et al., 2004). In general terms, MAX-DOAS can in principle give more information on the vertical distribution of absorbers than in-situ point source measurements. The measurement requires a less sophisticated optical system, less maintenance, and less power than comparable active DOAS systems. Typical instruments have moving telescopes or mirrors that allow the collection of scattered light from different viewing directions, defined by the elevation angle above the horizon, α, and the azimuth telescope pointing direction, β. Direct measurements are analyzed to yield slant column densities (SCDs) of trace absorbers integrated along the light path, and differential slant column densities (DSCDs) of trace gas species. DSCDs are determined by fitting all measurements ($\alpha<90°$) with zenith ($\alpha = 90°$) reference spectra. These spectra, called Fraunhofer references, are used to eliminate strong solar features in the incoming spectrum, and cancel out stratospheric absorptions, allowing DSCDs to contain mainly tropospheric absorptions (Hönninger et al., 2004).

The conversion of DSCDs into vertical column densities (VCDs) is not simple because, unlike for active DOAS, the exact path length for each DSCD is not known and depends on factors such as aerosol levels, clouds, albedo, the profile of the trace gases, and the location of the sun. The air mass factor (AMF) is defined as the ratio of the SCD over the VCD of a trace gas (Solomon et al., 1987; Perliski and Solomon, 1993). Radiative transfer models (RTMs) may be used to obtain AMFs based upon the above parameters. Under conditions with low aerosol, the AMF may be geometrically approximated by $1/\sin(\alpha)$ for a lower atmospheric absorber and scattering event above the absorbing layer (i.e. troposphere). However, since aerosols are present in most cases, this approximation is rarely valid, and an RTM should be used.

Spectroscopic instruments aboard satellites allow for the measurement of SCDs of trace gases (Bovensmann et al., 1999; Levelt et al., 2006). Using various algorithms, VCDs of trace gases can be determined after estimation of the AMF through radiative transfer modeling (Martin et al., 2002; Celarier et al., 2008). Satellites have the spatial advantage of obtaining global coverage, but have the temporal disadvantage of only obtaining a daily (OMI) or slightly better than weekly (SCIAMACHY) measurement for a given location on earth. The calculation of appropriate AMFs is a major task in the retrieval of tropospheric VCDs from satellite observations, as it requires a-priori information on clouds, aerosols, ground albedo, and trace gas profile. Satellite measurements of VCDs are also averaged over large pixel sizes and thus are challenged in the detection of changes on small spatial scales.

As MAX-DOAS and satellites yield comparable information on VCDs, intercomparison between the two methods is desirable. Recent studies have attempted to validate satellite measurements with ground-based measurements (Irie et al., 2009; Chen et al., 2009). The Dutch Aerosol and Nitrogen Dioxide Experiments for Validation of OMI and SCIAMACHY (DANDELIONS) study focused on urban areas and used geometrical considerations to convert MAX-DOAS DSCDs into VCDs (Brinksma et al., 2008; Celarier et al., 2008). Results from this study indicated that satellites underpredict NO_2 VCDs. Other studies have used RTMs to determine aerosol conditions and VCDs from MAX-DOAS in both rural and urban areas, using approaches that require a-priori assumptions (Wittrock et al., 2004; Heckel et al., 2005; Irie et al., 2008; Lee et al., 2009; Clémer et al., 2010).

In this paper, an original two-step approach to determine NO_2 VCDs from MAX-DOAS measurements is outlined, applied to a data set on a routine basis, and validated with other field measurements. The first step makes use of measured O_4 DSCDs and the RTM McArtim (Monte carlo Atmospheric radiative transfer inversion model) to obtain aerosol conditions for each MAX-DOAS measurement following the approach introduced by Li et al. (2010). This aerosol information is then input to McArtim for the calculation of NO_2 AMFs that are ultimately compared to the measured MAX-DOAS SCDs to obtain NO_2 VCDs. In addition to the NO_2 VCDs, aerosol optical depth (τ) values, aerosol layer heights (H_{aer}), and gas layer heights (H_{gas}) are also determined. A full description and comprehensive analysis of the methodology used is described in Wagner et al. (2011).

Complex meteorological phenomena imposed by lake breezes interacting with anthropogenic sources are known to modify the air quality in southern Ontario (Reid et al., 1996; Hastie et al., 1999; Sills et al., 2011). One goal of the 2007 Border Air Quality and Meteorology Study (BAQS-Met) was to examine such interactions, using a 3-week dataset collected in a rural region of southwestern Ontario,

supported by ground-based and aircraft-based measurements of trace gases and aerosols. The methodology outlined here for the determination of VCDs of NO_2 is validated against experimentally derived composite profiles of NO_2 (aircraft + ground measurements) collected during BAQS-Met, and compared to spatially and temporally coincident NO_2 VCDs determined from the satellite instruments, OMI and SCIAMACHY. The aerosol optical depth values are compared to spatially relevant OMI, MODIS, AERONET, and $PM_{2.5}$ measurements. Case studies are presented to demonstrate the ability of MAX-DOAS to detect the complex transport of NO_2 in this region.

2 Experimental

2.1 BAQS-Met Ridgetown supersite

Measurements were acquired at the Ridgetown site (Fig. 1), during the BAQS-Met field study, 20 June–10 July 2007. Ridgetown is a rural community with a population of ∼3500. The measurement site (42.45° N, 81.89° W), at an elevation of 202 m a.s.l., was located in an agricultural field at the north end of the University of Guelph (Ridgetown campus) away from the town center and direct anthropogenic influences. Surrounding sources (distance and direction) that can influence the site include a major highway, HWY 401 (4 km N), major refineries and chemical industry in Sarnia, ON (70 km NW), 2 major coal-fired power plants (65 km NW), Detroit/Windsor (100 km W), Cleveland, OH (100 km S) and the Golden Horseshoe (Toronto/Hamilton) urban area (200 km NE). Numerous urban areas and coal-fired power plants are also located in the Ohio valley region (100–500 km, S–SW). The site was 10 km from the north shoreline of Lake Erie.

2.2 The MAX-DOAS instrument and retrieval

The MAX-DOAS instrument used to measure scattered sunlight included a 1 m focal length Newtonian telescope (Sky Watcher, f/5) with a 20 cm primary mirror and a field of view of 0.06°. A stepper motor controlled the elevation angle (α), over the range from 0° (horizon) to 90° (zenith) with an error of ±0.2°. A fiber optic coupler in the telescope eyepiece focuses light into the fiber optic (2 m, 1000 µm diameter UV enhanced) that transfers light to a CCD spectrometer (Ocean Optics USB 2000^+, 323–471 nm, grating #7, 2400 lines mm^{-1}, 50 µm slit, UV4 upgrade, L4 lens), with 0.5 nm resolution. The spectrometer was housed in a Peltier cooling thermoelectric unit (Resonance Inc.) to achieve a stable temperature of 15 ± 0.2 °C. The spectrometer data was transferred to a PC via USB connection, while a custom LabVIEW program automated the measurement sequence including light level determination, integration times, collection and storage of averaged spectra, and movement of the telescope elevation angle by stepper motor prior to the next

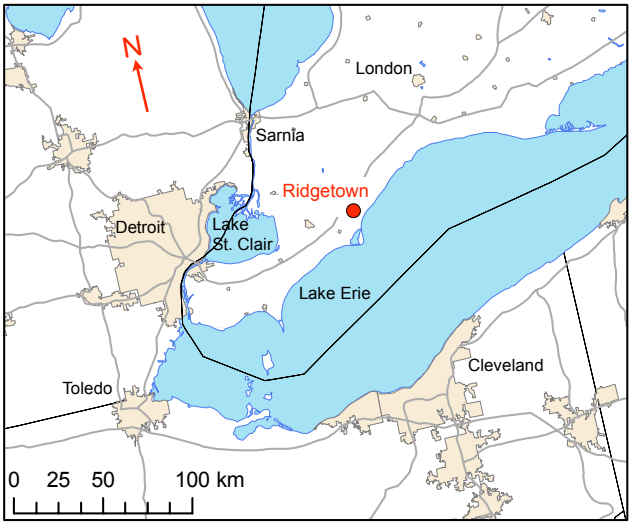

Fig. 1. BAQS-Met field study Ridgetown supersite and other areas of interest in southwestern Ontario and adjacent areas in the USA.

measurement. Every measurement began with an automatic determination of light level. This information was used to adjust the integration time of the measurement, ensuring that all measurements had an approximately equal level of signal. One complete cycle lasting approximately 30 min, consisted of a series of measurements with the following elevation angles (α): 90°, 30°, 10°, 6°, 4°, 2°. Each measurement typically consisted of 2000 averages with integration times ranging between 30–2000 ms, depending on light conditions. With the rationale of studying the passage of lake breeze fronts at the site, the MAX-DOAS telescope was pointed in the SW direction ($\beta = 235°$), parallel to the shoreline of Lake Erie.

Each spectrum was corrected by subtracting an electronic offset and dark noise spectrum. These corrected spectra were analyzed using the well-known DOAS technique (Plane and Smith, 1995; Platt, 1994; Platt and Stutz, 2008). A wavelength calibration using WinDOAS (Fayt and Roozendael, 2011) was performed by fitting a noon-time zenith spectrum ($\alpha = 90°$) taken on a clean day, henceforth called the Fraunhofer Reference Spectrum (FRS), to a high resolution solar spectrum (Kurucz et al., 1984) that was convolved with the instrument's slit function. A Ring spectrum (Grainger and Ring, 1962) was calculated from the FRS with DOASIS (Kraus, 2006). The NO_2 and O_3 (223 K and 243 K) absorption cross sections (Bogumil et al., 2003; Vandaele et al., 1998) were convolved using WinDOAS to match the instrument's resolution, while the O_4 (Greenblatt et al., 1990) cross section was interpolated. To determine the NO_2 DSCD for each spectrum, a 3rd order polynomial, the logarithm of the FRS, the Ring spectrum, convolved NO_2, convolved O_3 (223 K) and an additive polynomial (stray light) were fit to the logarithm of the corrected measurement spectrum

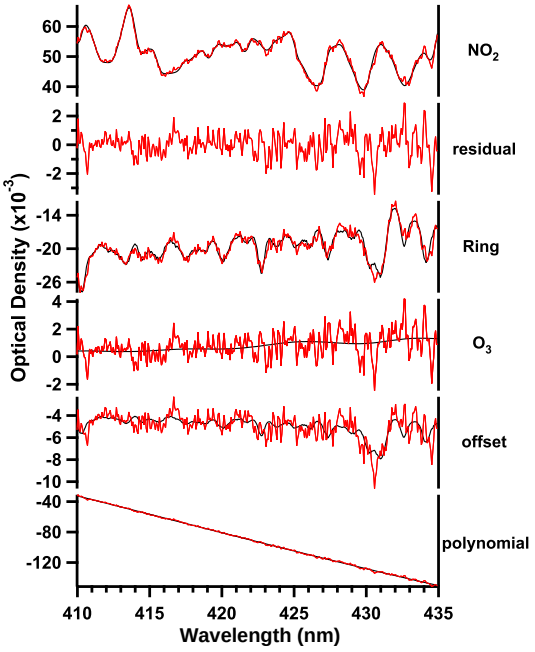

Fig. 2. NO_2 MAX-DOAS fit retrieval for a measurement with $\alpha = 4°$ on 20 June 2007, 09:46 EDT. This fit, performed between 410–435 nm, includes the NO_2 and O_3 absorption cross sections, plus a 3rd order polynomial, offset polynomial, FRS, and Ring. The residual of the fit is shown in the second panel. For each remaining panel the black line represents the DOAS fit, and the red line represents the DOAS fit plus the residual of the species examined.

using WinDOAS in the fit range 410–435 nm. All NO_2 fits were performed using a single FRS selected from a clean day during the field study. Figure 2 gives a sample fit for 20 June 2007, 09:46 EDT (Eastern Daylight Time = UTC-4). To determine the O_4 DSCD for each spectrum, a 4th order polynomial, the logarithm of the FRS, the Ring spectrum, interpolated O_4, convolved NO_2, convolved O_3 (223 K and 243 K) and an additive polynomial were fit to the logarithm of the corrected measurement spectrum in the fit range 355–385 nm. All O_4 fits were performed using daily FRS spectra selected from time periods closest to solar noon.

2.3 The active DOAS instrument and retrieval

Measurements of ground-based NO_2 were made using an active DOAS instrument that has been described in detail previously (McLaren et al., 2010). A retro-reflector was located 1.06 km SW of the site ($\beta = 235°$) at an elevation of 6 m a.g.l., giving a total path length of 2.12 km and an average beam height of 3.5 m a.g.l. The return beam was focused onto a 200 µm diameter quartz fiber optic (Ocean Optics), which coupled the light into a miniature spectrometer (Ocean Optics USB2000, Grating #10, 295–492 nm, 1800 lines mm^{-1}, 2048 element CCD, 25 µm slit, UV2 upgrade, L2 lens, resolution ~0.5 nm). Spectra were acquired with integration times between 150–350 ms and 4000 averages, for a time resolution of 7–13 min. Mercury lamp spectra were collected periodically for wavelength calibration and for convolving molecular reference spectra to the slit function of the spectrometer. Each ambient spectrum was corrected for electronic offset and dark noise. All spectra were fit using DOASIS (Kraus, 2006) in the range of 422–450 nm. The NO_2 fit scenario included a Xe lamp reference spectrum, convolved spectra of NO_2 (Vandaele et al., 1998) and O_3 (223 K) (Bogumil et al., 2003), and a 3rd order polynomial. The detection limit (3σ) for NO_2 was 1.1 ppb, determined by repetitive determination of a low concentration sample.

2.4 SCIAMACHY satellite measurements

The SCanning Imaging Absorption spectroMeter for Atmospheric CHartographY (SCIAMACHY) on board the European Space Agency's ENVIronmental SATellite (ENVISAT) (Bovensmann et al., 1999) measures Earthshine spectra from the UV to the NIR with a spectral resolution of 0.22–1.48 nm. It is operated in different viewing geometries, including nadir and limb. In nadir geometry (directed vertically down), the footprint of a single pixel is $\sim 30 \times 60\ km^2$. Global coverage of nadir measurements is achieved every 6 days. In standard operation mode, the measurement state alternates between limb geometry (directed horizontally, tangential to the Earth's surface), and nadir in such a way that limb measurements probe almost the same stratospheric air mass as subsequent nadir measurements.

From the Earthshine spectra measured by SCIAMACHY, total slant column densities of NO_2 are determined using the DOAS fitting technique. For the NO_2 fit in the spectral range 431–460 nm, appropriately convolved absorption cross sections of O_3, NO_2, O_4, H_2O, H_2O (liquid), and CHOCHO, Ring spectra accounting for vibrational and rotational Raman scattering, and a 5th order polynomial are included (Beirle et al., 2010). In order to extract tropospheric column densities, the stratospheric fraction is estimated and subtracted. This was done using the Reference Sector Method (Beirle et al., 2010). Stratospheric column densities are estimated over the remote Pacific and the remaining tropospheric residuals are corrected for longitudinal variations using the limb measurements of SCIAMACHY. For the conversion of tropospheric SCDs into VCDs of NO_2 (VCD_{SCIA} values), tropospheric AMFs are calculated via the RTM McArtim (Deutschmann et al., 2011), assuming a fixed tropospheric profile with 80 % of the tropospheric NO_2 within a constant boundary layer with a height of 1 km (Chen et al., 2009).

2.5 OMI satellite measurements

Onboard the Aura satellite, the Ozone Monitoring Instrument (OMI) is a nadir-viewing spectroradiometer that uses a 2-D CCD to simultaneously measure the Earthshine spectra in the UV-Vis range from 270–500 nm (Levelt et al., 2006).

Specifically, OMI measures in three broad spectral regions (UV-1, UV-2, Vis) with a spectral resolution between 0.45 and 1.0 nm. It provides global coverage daily with a pixel size of $13 \times 24\,km^2$ at nadir increasing to $\sim 40 \times 160\,km^2$ at the two ends of the scan line.

The present study uses the NASA standard product (overpass version) of the VCD of NO_2 (VCD_{OMI}) obtained from the NASA Aura Validation Data Centre (AVDC) website (NASA, 2010b). From the Earthshine spectra measured by OMI, total slant column densities of NO_2 are determined using the DOAS fitting technique. For the NO_2 fit in the spectral range 405–465 nm, appropriately convolved absorption cross sections of O_3 (Burrows et al., 1999), NO_2 (Vandaele et al., 1998), H_2O (Harder and Brault, 1997), a Ring spectrum (Chance and Spurr, 1997) accounting for vibrational and rotational Raman scattering, and a cubic polynomial are included. To convert these SCDs into VCD_{OMI} values, different types of AMFs were calculated using geographically gridded ($2.5° \times 2.0°$) annual mean NO_2 profiles (GEOS-CHEM was used for tropospheric, and the Goddard Chemical Transport model was used for stratospheric profiles (Bucsela et al., 2006)). Details of the algorithm used for the retrieval of the VCD_{OMI} may be found in (Boersma et al., 2001; Bucsela et al., 2006; Celarier et al., 2008; Wenig et al., 2008).

2.6 MODIS and OMI aerosol products

The MODerate resolution Imaging Spectroradiometer (MODIS) provides the aerosol optical depth over portions of the continents and over oceans, from two satellites (Terra, Aqua). Daily level 2 data products provide a spatial resolution of a 10×10 1-km pixel array (nadir). Two MODIS aerosol level 2 data products, collection 5, MOD04_L2 and MYD04_L2, from the Terra and Aqua satellites respectively, are available from the Level 1 and Atmospheric Archive and Distribution System (LAADS) website (NASA, 2010a). Only those data products that overlapped Ridgetown were used. All MODIS aerosol optical depth values were found at $\lambda = 550$ nm, and had a maximum sensitivity over land of $0.05 \pm 15\,\%$ (Levy et al., 2007). OMI aerosol optical depth (τ) values were taken from the NASA AVDC (NASA, 2010b). The OMAERUV L2 product was selected ($\lambda = 388$ nm) for a satellite overpass of Ridgetown. Information on this OMI near-UV retrieval algorithm may be found in Torres et al. (1998).

2.7 AERONET aerosol products

AErosol RObotic NETwork (AERONET) aerosol optical depth (τ) values were taken from direct solar measurements using CIMEL sun photometers at two measurement sites (Kellogg, Michigan, USA, 42.41° N, 85.37° W, 293 m a.s.l., and Egbert, Ontario, Canada, 44.23° N, 79.75° W, 264 m a.s.l.) (NASA, 2010c). All τ values used have an uncertainty of ~0.01 to 0.02 ($\lambda = 340$ and 380 nm) and were AERONET Version 2.0, Level 2.0 – quality assured data, meaning they were pre- and post-field calibrated, automatically cloud-cleared and manually inspected. Details regarding the AERONET network, and the procedures used to calculate aerosol optical depths may be found in (Dubovik and King, 2000; Holben et al., 1998, 2001).

2.8 Additional supporting measurements

The NO_2, SO_2, and $PM_{2.5}$ were measured at ground level using a chemiluminescence NO_x analyzer with Mo converter (Thermo Model 42C), trace level pulsed fluorescence SO_2 analyzer (Thermo Model 43C-TL), and Tapered Element Oscillating Microbalance (TEOM) ambient $PM_{2.5}$ monitor (R & P Model 1400B with sample equilibration system), respectively. These measurement devices were located in the Ontario Ministry of the Environment's mobile particulate laboratory at the Ridgetown site. Measurements of NO_2 and other meteorological measurements were also made onboard the NRC Twin Otter Aircraft that was dedicated to the BAQS-Met field campaign. The NO_2 measurements were performed with a chemiluminescence NO_x instrument (TECO 42S) retrofit with a photolytic converter, for measurement of "true" NO_2 ($\pm 15\,\%$), with a detection limit of 60 pptv (3σ, 1 min). Details on the aircraft campaign measurements are provided in Hayden et al. (2011).

The scanning LIDAR facility (RASCAL – Rapid Acquisition SCanning Aerosol LIDAR), capable of fast azimuth and elevation scanning of the lower troposphere, was present at the Ridgetown site. A full description of its operation is given elsewhere (Strawbridge et al., 2004). It was primarily used for the comparison of boundary layer heights to H_{aer} and H_{gas}, as described in Sect. 4.3.

3 Methodology for determining τ and NO_2 VCDs from MAX-DOAS

A full description of the methodology used for determining aerosol optical depths (τ) and NO_2 VCDs from the MAX-DOAS measurements is included in the Supplemental Material. A short description, summarized in Fig. 3, is given here. The methodology includes experimental retrievals (Fig. 3 – field measurements) of the DSCDs of NO_2 and O_4 from the MAX-DOAS measurements, as described previously. Wagner et al. (2004) introduced the concept of using the O_4 absorption to retrieve aerosol profiles (Frieß et al., 2006; Li et al., 2010; Wittrock et al., 2004). The O_4 species is found in greatest amounts close to ground level, the result being that O_4 DSCDs are very sensitive to changes in light path due to varying levels of aerosols. A radiative transfer model (Fig. 3 – forward modeling), McArtim (Deutschmann et al., 2011), calculated the DAMFs of O_4 at all elevation angles as a function of the solar and experimental conditions at Ridgetown.

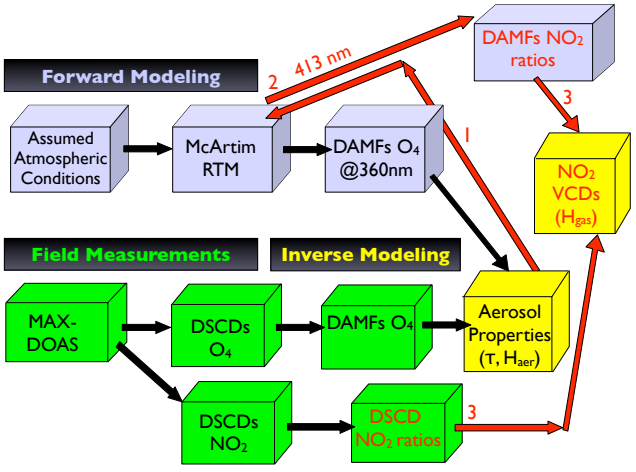

Fig. 3. Flowchart of methodology for determination of NO_2 VCDs and aerosol properties from MAX-DOAS measurements, RTM and inverse modeling. Measurements in green boxes represent products obtained from direct MAX-DOAS measurements in the field, while parameters and products shown in the grey boxes represent modeled quantities and results only. The quantities in the yellow boxes are obtained from inverse modeling.

The RTM presumes that the aerosols are confined to a box of height H_{aer}. H_{aer} is equivalent to the boundary layer height (BLH) if aerosols are 100% confined to the boundary layer (also see (Zieger et al., 2011)), although this is rarely the case. A comprehensive set of O_4 DAMFs was catalogued in a look up table. A MATLAB routine (Fig. 3 – inverse modeling) was used to minimize the difference between O_4 DAMFs in the look-up and O_4 DAMFs calculated by dividing the measured DSCDs by an estimated VCD. This minimization yields τ, henceforth named τ_{RTM}, and H_{aer}, which describe the aerosol conditions for each cloud-free measurement series.

The aerosol conditions were input to McArtim in the determination of NO_2 VCDs. The NO_2 DAMFs are a function of both the aerosol conditions and the vertical profile of NO_2. The vertical profile of NO_2 in the troposphere was assumed to be a homogeneous layer of thickness H_{gas}. The contribution of stratospheric NO_2 was removed by subtracting the SCD_{90} in each measurement series from other SCD_α values ($\alpha = 2°$, 4°, 6°, 10°, 30°) in the series. McArtim was used to calculate a comprehensive set of "box" NO_2 DAMFs in a lookup table. A minimization of differences between the $DSCD_{meas}$ ratios and the $DAMF_{ratios}$ in the look-up, yielded the best values of H_{gas} and VCD_{NO_2}, henceforth known as VCD_{RTM}. This inversion was performed for all complete elevation sequences with SZA <80°. NO_2 sequences with deviations of more than 2× $DSCD_\alpha$ between DSCDs for subsequent elevation angles were eliminated. Results with non-convergent fits were not defined.

Our method assumes that both aerosols and NO_2 are confined to homogeneous layers of height H_{aer} and H_{gas} respectively. More generally, one may model more complex scenarios in which fractions, f_{aer} and f_{gas} of total tropospheric aerosols and NO_2 are confined to ground layers, with remaining fractions of aerosols ($1-f_{aer}$) and NO_2 ($1-f_{gas}$) modeled as exponential decay functions above the homogeneous layer. In this study, a sensitivity analysis showed that the values of τ and VCD_{RTM} are largely insensitive to the chosen values of f ($f \geq 0.5$), however the retrieved values of H_{aer} and H_{gas} are strongly a function of f. A more comprehensive description, sensitivity analysis, and further validation of the method outlined here may be found in Wagner et al. (2011).

For the sake of comparison, we also present geometrically approximated VCDs of NO_2, where $VCD_{GEO} = DSCD_{30}$, as shown in the Supplemental Material. For the sake of comparing to other measures of VCD in this paper, and to be consistent with other literature, a criterion was applied such that VCD_{GEO} ($\alpha = 30°$) and VCD_{GEO} ($\alpha = 10°$) must agree to within 15% to be retained, eliminating points affected by horizontal inhomogeneites, aerosols, or clouds (Brinksma et al., 2008; Celarier et al., 2008).

4 Results and discussion

4.1 Aerosol optical depth/aerosol extinction coefficient

Figure 4 displays the O_4 DSCD values at Ridgetown for the entire field campaign, under cloud-free conditions. The O_4 DSCDs typically increase with decreasing elevation angles, indicative of a tropospheric absorber, such as on 20, 22, 23, 29 June and 2 and 7 July. However, in several cases (parts of 25, 26, 27 June, and 4, 5, 9, and 10 July) there appears to be little dependence of the DSCDs on elevation angle. This phenomenon occurs when high levels of aerosol and/or clouds are present and thus the light path from the last scattering event to the detector becomes effectively equal, regardless of the elevation angle of the observation. As only cloud-free conditions are presented here, the effect is largely due to the presence of aerosols. As such, when qualitatively comparing aerosol levels, days such as 20 June appear to contain low aerosol extinction, while days such as 9 July, contain high aerosol extinction.

In order to assess conditions on a more quantitative level, the aerosol optical depth (τ_{RTM}) for each measurement series was determined at 360 nm, as described in Sect. 3 and the Supplemental Material. The τ_{RTM} varied from 0.05 to 2.93, with a mean and a median value of 0.41 and 0.46 respectively (Fig. 5). The average relative error of each τ_{RTM} value was estimated at 26 % (Wagner et al., 2011). The τ_{RTM} values were compared to those τ values found from satellite measurements (τ_{MODIS}: $\lambda = 550$ nm, τ_{OMI}: $\lambda = 388$ nm), and AERONET ground-based measurements at Egbert and Kellogg (τ_{EGB}, τ_{KEL}, $\lambda_{avg} = 360$ nm for each location). Satellite measurements are only optimally available on a daily basis. The comparison was limited due to the different wavelengths

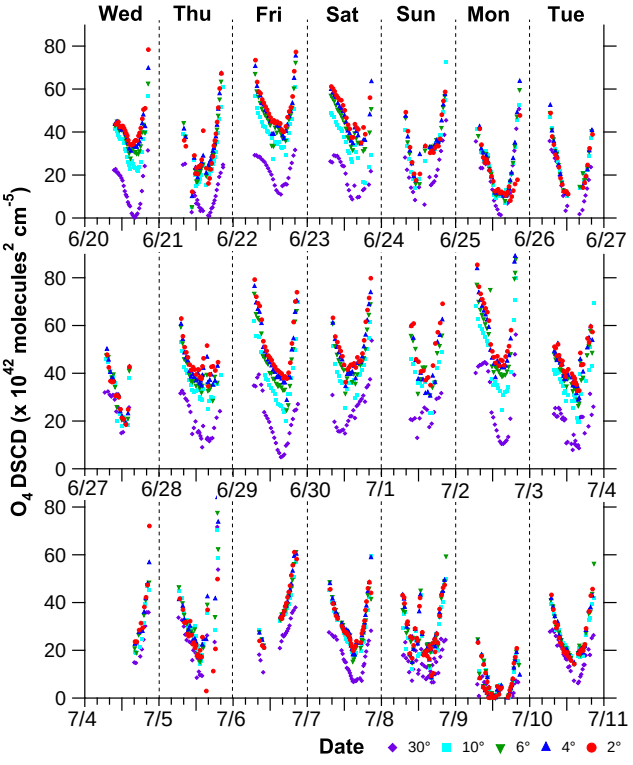

Fig. 4. O_4 DSCDs for cloud-free conditions during the BAQS-Met campaign at the Ridgetown supersite. Major ticks represent 12 midnight and 12 noon EDT, while minor ticks indicate every 4-h increment.

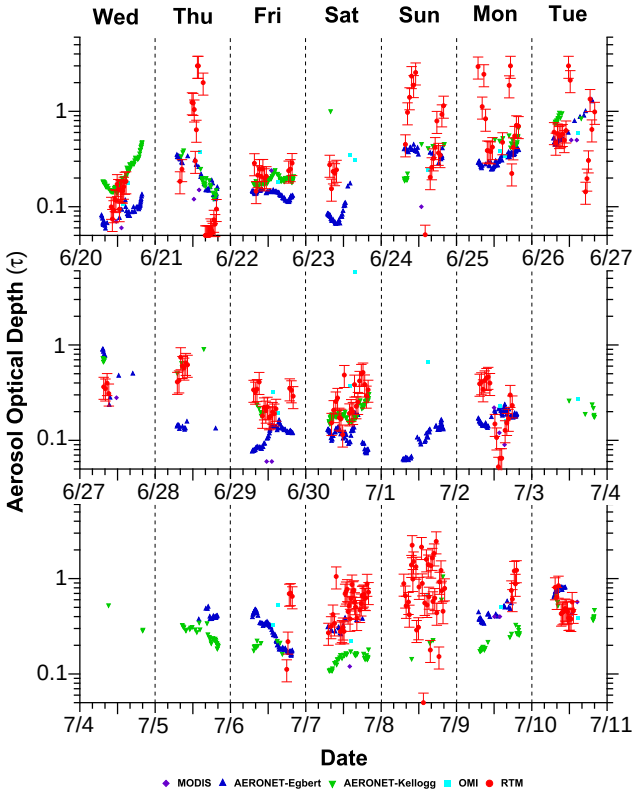

Fig. 5. Aerosol optical depth for the entire BAQS-Met campaign. For AERONET locations (Egbert, Kellogg) $\lambda_{avg} = 360$ nm, for coincident satellite measurements (OMI $\lambda = 388$ nm, MODIS $\lambda = 550$ nm), and for the MAX-DOAS-RTM values at Ridgetown, $\lambda = 360$ nm.

used (particularly for τ_{MODIS}) and the fact that the satellites only provide 1 or 2 comparison points daily. Although the measurements are made at similar λ for the AERONET locations, they are relatively far from Ridgetown (Egbert ~320 km NE, Kellogg ~330 km W), yet Ridgetown is approximately central between the two locations. The above factors limit the ability to make direct comparisons of τ_{RTM} at Ridgetown, yet the values of τ_{RTM} do lie within the range of the other measurements, as might be expected during times when the high aerosol loading is associated with regional pollution events that affect eastern North America over large spatial distances. Such regionally polluted conditions were observed from 24–27 June and 8–10 July.

Spatially, it would be better to compare the τ_{RTM} values with aerosol levels measured directly at Ridgetown. Although another measure of τ is not available at the site, $PM_{2.5}$ mass was measured. When the $PM_{2.5}$ was compared to the corresponding τ_{RTM} values, a low level of correlation was found ($R^2 = 0.068$). This is not surprising since $PM_{2.5}$ is a ground point-source measurement of particulate mass, while τ_{RTM} represents an integrated column quantity of aerosol extinction. A more appropriate comparison of the aerosol properties may be done by examining the aerosol extinction coefficient ($E = \tau_{RTM}/H_{aer}$, see Supplement).

Figure 6a shows the time series comparing the aerosol extinction coefficient and the $PM_{2.5}$ measured at Ridgetown. A correlation plot for these two related properties is shown in Fig. 6b using data from the entire study. Both panels show that there is a high degree of correlation between aerosol extinction and $PM_{2.5}$ ($R^2 = 0.75$) (also see Zieger et al., 2011). This improved correlation implies that MAX-DOAS observations are sensitive to the total column amount of aerosol, in comparison to the $PM_{2.5}$ measurement that is sensitive to the concentration of aerosol. It also implies that temporal variations in the aerosol layer height, H_{aer}, are likely significant at Ridgetown.

Recent studies have compared local PM_{10} and $PM_{2.5}$ measurements to τ values determined from MODIS (Chu et al., 2003; Engel-Cox et al., 2004, 2006; Gupta and Christopher, 2008; Kacenelenbogen et al., 2006; Pelletier et al., 2007; Schaap et al., 2009; Wang and Christopher, 2003). The extent of correlation they found between τ_{550} (MODIS) and $PM_{2.5}$ varied, with R^2 values ranging from 0.27 to 0.60. This range is not entirely surprising as variations in local meteorology, differing aerosol composition, and the distribution of the aerosol layer(s) may all play roles in this relationship.

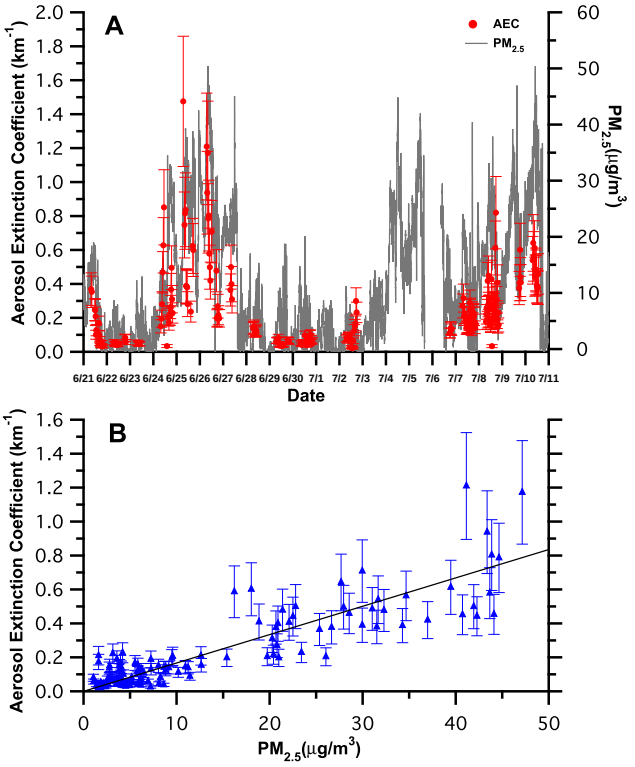

Fig. 6. Top panel **(A)** – aerosol extinction coefficient (red) and $PM_{2.5}$ (grey) at Ridgetown. Bottom panel **(B)** – $PM_{2.5}$ vs. aerosol extinction coefficient – Ridgetown. Slope of the trend line (y-intercept zero forced) = 16 ± 1 m^2 g^{-1}, $R^2 = 0.75$.

In particular if aerosols are concentrated in the boundary layer, and the boundary layer height is highly variable, a poor relationship between τ and $PM_{2.5}$ would be expected. If the boundary layer height is known, this correlation may be greatly improved through calculation of E. For example, Koelemeijer et al. (2006) found that there was a better correlation ($R^2 = 0.59$) between $PM_{2.5}$ measurements and the modified aerosol extinction from MODIS, E^*:

$$E^* = \frac{\tau}{\mathrm{BLH} \cdot f(\mathrm{RH})} \quad (1)$$

with BLH being the boundary layer height, and f(RH) a factor that takes into account the hygroscopic growth of aerosols, as opposed to directly comparing hourly $PM_{2.5}$ and τ ($R^2 = 0.38$). Their result implied that most of the aerosol was found within the boundary layer, whose height is variable, preventing an easy direct measurement of aerosol mass through satellite derived quantities.

Further studies have determined aerosol extinction coefficients and aerosol optical depths from MAX-DOAS O_4 measurements and radiative transfer modeling, and compared them to PM_{10}, LIDAR calculated extinction coefficients, and aerosol optical depths from sky radiometers. Irie et al. (2008) compared extinction coefficients from MAX-DOAS-RTM inversions run at 476 nm with LIDAR calculated extinction coefficients (slope = 1.01, $R^2 = 0.85$) and compared τ values found from these MAX-DOAS-RTM inversions with τ values from a sky radiometer. Both comparisons agreed to within 30 % for values determined from ground level to a height of 1 km. Lee et al. (2009) compared extinction coefficients found from a MAX-DOAS-RTM inversion run at 356 nm to LIDAR calculated extinction coefficients ($R^2 = 0.70$), and they agreed to within 50 %, while a comparison between MAX-DOAS-RTM derived extinction coefficients and PM_{10} also showed a relatively good correlation. Our results are consistent with these studies.

4.2 Validation of VCD_{RTM} against vertical measurements of NO_2

In order to validate our method for deriving NO_2 VCDs using MAX-DOAS and RT calculations, we derived comparative VCDs of NO_2 from a composite profile of ground-based and aircraft-based NO_2 measurements in the vicinity of Ridgetown during the same time frame as the MAX-DOAS measurements. The composite profiles included ground-based NO_2 measurements at Ridgetown via active DOAS, vertical measurements of NO_2 when the aircraft was in the vicinity of Ridgetown, and suitable estimates of NO_2 in the free troposphere above the maximum height of the aircraft. Suitable temporal and spatial overlapping data were found for one day, 26 June 2007. Two composite profiles of NO_2 were derived in the late afternoon on this day, concurrent with two MAX-DOAS measurements and their corresponding VCD_{RTM} determinations. The vertical profiles can be split into three sections. Section 1 extends from the ground to the top of the boundary layer, where NO_2 was determined by ground-based and aircraft measurements of NO_2 close to Ridgetown. Section 2 corresponds to the region of the free troposphere from the top of the boundary layer to the maximum height at which aircraft measurements were available. Section 3 corresponds to the free troposphere above the maximum aircraft height, where a constant NO_2 mixing ratio of 50 ppt was assumed (Blond et al., 2007). The boundary layer height in the afternoon, 797±45 m a.g.l., was determined by potential temperature profiles measured by the aircraft.

Figure 7a shows the flight path on 26 June where the NO_2 mixing ratio is displayed as a function of time and location. The position of the aircraft for every 20 min interval is also shown. Figure 7b shows the altitude profile for the flight including ascending, descending, and stable height time periods. In general, the degree of spatial homogeneity in NO_2 increases with height, in the absence of elevated plumes sources. Our criteria for inclusion of data in the composite profile reflected this; the aircraft had to be within 30 km of Ridgetown over land for boundary layer measurements, within 50 km of the site for heights from the top of the boundary layer to 1400 m a.g.l., and within 140 km of the site for heights between 1400 and 3000 m a.g.l. (Fig. 7). Figure 8

Table 1. Comparison of RTM and composite VCDs of NO_2 on 26 June 2007.

Point	Time (EDT)	VCD^*_{COMP} (10^{15} molec cm^{-2})	VCD^*_{RTM} (10^{15} molec cm^{-2})	Error (10^{15} molec cm^{-2})	VCD^*_{RTM} vs. VCD_{COMP}
1	17:25–17:46	3.06 ± 1.22	2.59 ± 0.44	-0.47	
2	17:52–18:15	3.18 ± 1.22	3.50 ± 0.44	0.32	
Mean		3.12 ± 0.86	3.04 ± 0.31	0.40	0.98 ± 0.29
RMSE				0.40	

* All uncertainties are standard (1σ).

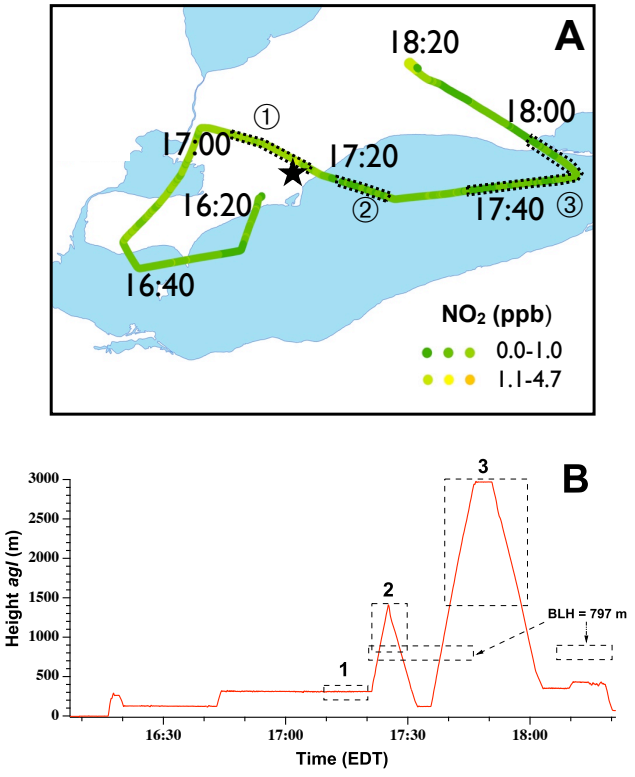

Fig. 7. Flight path on 26 June 2007. Panel **(A)** shows the NO_2 mixing ratios and the aircraft location every 20 minutes. Panel **(B)** shows the aircraft elevation and BLH (a.g.l.) as a function of time. The numbered sections show the locations, elevations, and approximate mixing ratios used for constructing the composite NO_2 profiles. The Ridgetown supersite location is starred.

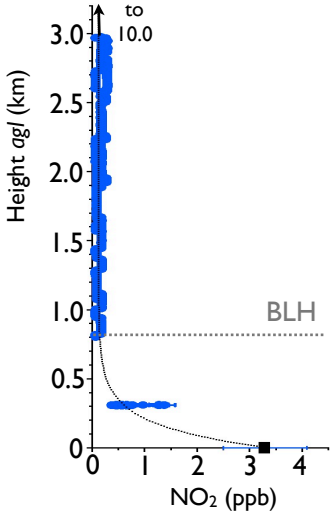

Fig. 8. The NO_2 concentration profile used to construct the composite NO_2 VCDs on 26 June 2007. Blue circles represent NO_2 aircraft measurements, while the black square represents the ground-based NO_2 by active DOAS. The boundary layer (BLH) is marked with the horizontal dashed line.

displays a sample profile. Error bars in the x dimension represent uncertainties in the NO_2 mixing ratios. The boundary layer was found to be inhomogeneous on this afternoon. Mixing ratios of NO_2, measured when the aircraft penetrated into the boundary layer over land close to Ridgetown were much lower than values measured at the ground. For this reason, Sects. 1 and 2 were combined for the purposes of mathematical fitting. The NO_2 profile was assumed to decay exponentially from the ground up through Sects. 1 and 2.

For all sections, number densities of NO_2 were calculated as a function of height accounting for the non-linearity of pressure and temperature. The total tropospheric VCD of NO_2, henceforth called the composite VCD (VCD_{COMP}), is then obtained using Eq. (2):

$$VCD_{COMP} = \int_0^{BL} n_{1,NO_2} dz + \int_{BL}^{TOAc} n_{2,NO_2} dz + \int_{TOAc}^{10\,km} n_{3,NO_2} dz \quad (2)$$

where n_{NO_2} is the number density of NO_2 for Sects. 1, 2, 3, and TOAc represents the top of available aircraft measurements.

The two VCD_{COMP} values determined on this day are compared to the corresponding VCD_{RTM} values, coincident in time, in Table 1. The uncertainties in the VCD_{COMP} arise from several sources. For Sects. 1 and 2, the uncertainty in the exponential fit of NO_2 vs. height was primary. For Sect. 3 the uncertainty in the NO_2 mixing ratio (50 ppt) was assumed to be $\pm 100\%$. Uncertainties due to spatial and temporal differences between the aircraft measurements and the

MAX-DOAS column also exist but are not considered here as they cannot be determined. The uncertainty of VCD_{RTM} (0.44×10^{15} molec cm^{-2}) was based on the standard deviation of VCD determinations at different elevation angles (see Supplemental Material).

The mean value of VCD_{COMP} in Table 1 is $3.12\pm0.86\times10^{15}$ molec cm^{-2}, which is reasonable for a rural region (Heland et al., 2002; Irie et al., 2009; Ladstätter-Weißenmayer et al., 2003). The mean value of VCD_{RTM} was $3.04\pm0.31\times10^{15}$ molec cm^{-2}. The ratio VCD_{RTM}/VCD_{COMP}, is 0.98 ± 0.29, which is not statistically different from 1.0. The mean bias in the comparison is -0.08×10^{15} molec cm^{-2}, again not statistically different from zero. Although we have only compared a limited number of points, this comparison serves as a validation of the method outlined in this paper for the determination of VCDs. There is no evidence of a bias in the determination of VCD using this method at the moderate NO_2 column levels that existed during the comparison.

4.3 Comparison of boundary layer heights and retrievals of H_{aer} and H_{gas}

Although the focus in this study was not the determination of accurate boundary layer heights (BLHs), it is instructive to compare the retreived aerosol and gas heights, H_{aer} and H_{gas}, and BLHs determined by LIDAR backscatter measurements. LIDAR data was available on 6 days (08:00–16:00 EDT), simultaneous with MAX-DOAS-RTM determinations. There were 25 simultaneous determinations of BLH, ranging from 0.1 km–2.0 km a.g.l., from early morning to late afternoon respectively. Figure 9 shows the correlations between the retrieved heights and the BLH, zero-forced since the intercepts were not statistically different from zero. The correlation coefficients are low ($R^2 = 0.17$ for H_{aer}; 0.08 for H_{gas}), indicating that the retrievals only capture a small amount of the variance associated with the backscatter BLHs. It is also apparent that the values of H_{aer} are significantly higher than the BLHs, by almost a factor of 2, and that the H_{gas} values are significantly lower than the BLHs, by a factor of 2. The correlation coefficients are improved by applying a more rigid set of criteria for inclusion of data pairs as shown in Wagner et al. (2011); however the slopes still remain much the same, which requires an explanation. The H_{aer} slope of 1.92 ± 0.21 likely results from the fact that aerosols are not exclusively confined to the boundary layer, especially in early morning periods when significant amounts of aerosols left over from the previous day can exist in the residual layer, as was directly observable in LIDAR images. This is partly attributable to the longer lifetime of aerosols in the atmosphere, compared to NO_x, and partially attributable to the ubiquitous secondary source of aerosols throughout the atmospheric column. On the other hand, the sources of NO_x are predominantly surface-based within the boundary layer, which combined with its shorter lifetime than aerosols gives

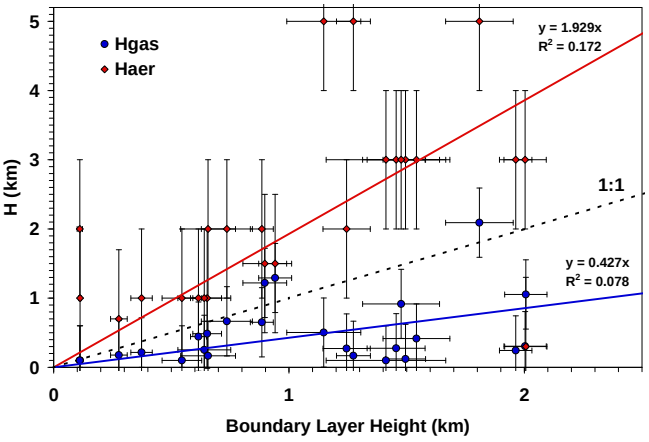

Fig. 9. Correlation between MAX-DOAS-RTM retrieved layer heights and boundary layer heights determined by LIDAR backscatter determinations.

rise to a negative gradient of NO_2 in the boundary layer (see Fig. 8). When modeled as a homogeneous layer, the H_{gas} height is lower than the BLH (slope = 0.43 ± 0.08); however an accurate VCD can still be obtained. A sensitivity analysis was performed in which the fraction of NO_2 (f_{gas}) and aerosols (f_{aer}) confined to the homogeneous layer were allowed to vary from 0.5 to 1.0. The τ_{RTM} values were found to agree quite well ($\pm2\%$) for moderately and highly polluted days, and less so on low aerosol days with a maximum difference of 21% on a very clean day ($\tau \sim 0.05$). The variance in VCD_{RTM} was $\pm6\%$ under all aerosol conditions tested in the sensitivity study. Thus accurate values of τ and VCD are still obtained using the current methodology. If this method is to be used for accurate determinations of BLH, then time dependent values of f_{aer} and f_{gas} would be needed. A more thorough discussion of the sensitivity of the retrievals to f_{aer} and f_{gas} is given elsewhere (Wagner et al., 2011).

4.4 Comparison between VCD_{RTM} and satellite VCDs of NO_2

Figure 10 displays all tropospheric VCDs of NO_2 for the Ridgetown site throughout the study. The VCD_{RTM}, VCD_{GEO}, and VCD_{COMP} (26 June) are shown, along with the satellite-derived measures, VCD_{OMI} and VCD_{SCIA}. Only 9 VCD_{SCIA} measurements were available during the study period due to the limited temporal sampling of the ENVISAT satellite. There were 31 measurements from the OMI instrument on the Aura satellite as it provides daily global coverage with successive orbits separated by 100 min providing one or two measurements per day at a specified location. To facilitate comparisons between VCD_{RTM} and $VCD_{satellite}$, measurements were paired only when the two measurements were made within one hour of each other. Only one comparison pair was available for SCIAMACHY while 8 comparisons were available for the OMI instrument.

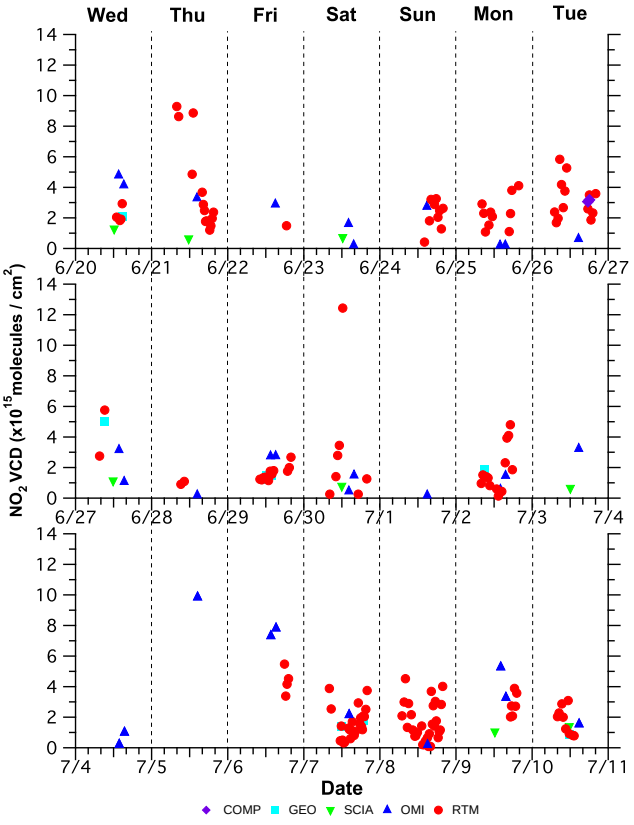

Fig. 10. Comparison of all NO_2 tropospheric VCDs at Ridgetown derived from aircraft/ground, satellite, and MAX-DOAS-RTM measurements.

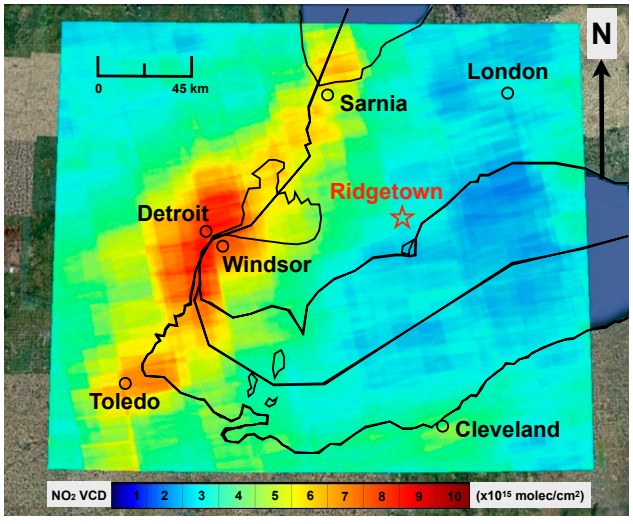

Fig. 11. Averaged OMI tropospheric NO_2 VCDs for the intensive field study period (20 June–10 July 2007) in southwestern Ontario. Ridgetown supersite is starred.

The statistical comparison is provided in Table 2, where all VCDs are compared to VCD_{RTM}. The comparison indicates that the VCDs derived by satellite were higher than those of the VCD_{RTM}. Presuming a proportionate error, the two satellites determinations are about 50 % higher than VCD_{RTM}, but only statistically so for the OMI instrument. The proportionate error for OMI was determined in two ways: (i) the ratio of the averages, VCD_{OMI}/VCD_{RTM}, and (ii) the slope of the regression of VCD_{OMI} vs. VCD_{RTM}, with the y-intercept forced to zero (intercept was equal to zero within error). If one presumes a constant bias in the satellite retrievals, the mean bias is $+0.91\times10^{15}$ molec cm^{-2} for OMI and $+0.48\times10^{15}$ molec cm^{-2} for SCIAMACHY. Our results do not provide sufficient statistical evidence as to whether the retrieval error is proportionate or absolute. However, it should be noted that the total VCDs experienced at this rural site are relatively small. Thus the large apparently relative overprediction for the satellite retrievals (+50%) is not necessarily a result that is transferable to more polluted regions with higher VCDs of NO_2.

Earlier studies (Brinksma et al., 2008; Celarier et al., 2008; Chen et al., 2009; Irie et al., 2009) found various satellite-derived NO_2 VCDs to be substantially lower than MAX-DOAS derived NO_2 VCDs. It should be noted that in those studies the MAX-DOAS VCDs were geometrically approximated (similar to VCD_{GEO}), and the distinction from a full MAX-DOAS with radiative transfer derived VCD (VCD_{RTM}) should be taken into account in all these studies. Our observation of satellite VCDs with a positive bias compared to VCD_{RTM} and VCD_{COMP} is in contrast to the earlier studies. One possible explanation for this is that previous comparisons have frequently focused on urban and suburban areas where average NO_2 VCDs were significantly higher. For example, the VCD of NO_2 ranged from $0.5–5\times10^{16}$ molec cm^{-2} during DANDELIONS at Cabauw, Netherlands (Brinksma et al., 2008; Celarier et al., 2008) with a median of $\sim1.5\times10^{16}$ molec cm^{-2}, whereas the VCD range in the current study is $0.01–1.25\times10^{16}$ molec cm^{-2} with a median of 2.00×10^{15} molec cm^{-2}. In that study, the MAX-DOAS instruments measured very high NO_2 VCDs in a polluted region, which could not be completely captured by the satellite, due to the regional averaging implicit with a large pixel size. Under such conditions, the satellite will measure lower values than the more localized in situ measurement. The opposite would be true in this study. Being situated in a rural region, the local measurements of NO_2 made by MAX-DOAS and the aircraft are relatively low. In contrast, the large pixel area coverage of the satellite instruments (OMI – 13×24 km^2, SCIAMACHY – 30×60 km^2) will be higher than the local measurement when the pixel is impacted by surrounding urban areas, such as may occur when prevailing westerly winds carry pollutants from Windsor-Detroit towards Ridgetown. If a significant amount of a given pixel lies within a position west of Ridgetown, it may be detecting NO_2 from this urban outflow, and thus overestimate the actual NO_2 present at the site (see Fig. 11).

Table 2. Comparison of various NO_2 VCDs to the values of VCD_{RTM}.

	OMI AURA*	SCIAMACHY ENVISAT	Geometric Approximation*	Aircraft Composite*
Number of Data Pairs, N	8	1	10	2
$\overline{VCD}_{measured}$ ($\times 10^{15}$ molec cm^{-2})	2.67 ± 0.18	1.39	1.88 ± 0.05	3.12 ± 0.86
$\overline{VCD}_{RTM}$ ($\times 10^{15}$ molec cm^{-2})	1.76 ± 0.16	0.92 ± 0.44	2.05 ± 0.14	3.04 ± 0.31
$\overline{VCD}_{measured}/\overline{VCD}_{RTM}$	1.52 ± 0.17	1.5	0.92 ± 0.07	1.02 ± 0.30
Slope (forced zero intercept)	1.47 ± 0.20	N/A	0.88 ± 0.04	1.01 ± 0.13
Correlation, R	0.63	N/A	0.97	0.98
Mean Absolute Error ($\times 10^{15}$ molec cm^{-2})	1.12	0.48	0.30	0.40
RMSE ($\times 10^{15}$ molec cm^{-2})	1.33	N/A	0.41	0.40
Mean Bias ($\times 10^{15}$ molec cm^{-2})	+0.91	+0.48	−0.17	+0.08

* All uncertainties are standard (1σ).

Additionally, the satellite retrievals used here do not consider aerosol conditions or temporal changes in the NO_2 profile in their fitting routines. Uncertainties in these parameters could lead to uncertainties in the overall satellite-derived VCD, and with low levels of NO_2, this may lead to large relative uncertainties in these VCDs.

Also included in Table 2 is a statistical comparison of VCD_{GEO} to VCD_{RTM}, where the conservative selection criteria for inclusion was fulfilled, namely that the values of geometrically approximated VCDs for elevation angles of 10° and 30° in the same measurement series agreed to within 15 %. The selection criteria is quite limiting and is fulfilled for 10 data pairs only, as seen in the table. Similar criteria has been used in past studies to ensure that the VCDs determined by the geometric approximation are not heavily influenced by aerosols, thus making them appropriate for comparison to satellite measures (Brinksma et al., 2008; Celarier et al., 2008). Although our method with full radiative transfer is favored, the VCD_{GEO} comparison allows benchmarking to previous literature. The comparison indicates that VCD_{GEO} is lower than VCD_{RTM} by 8–12 %, presuming a proportional error, or with a mean bias of -0.17×10^{15} molec cm^{-2}, presuming an absolute error. Since both of these VCDs are derived either partly or entirely from the same set of MAX-DOAS measurements, they have nearly identical measurement times, and compared pairs show a high correlation between VCD_{GEO} and VCD_{RTM} ($R^2 = 0.97$).

The average NO_2 VCD retrieved from OMI measurements during the study period (20 June–10 July 2007) for the BAQS-Met study domain is mapped on a 0.002° × 0.002° grid, as described in Wenig et al. (2008), in Fig. 11. The highest VCDs are seen over the metropolitan area of Detroit/Windsor with average VCDs up to $\sim 1 \times 10^{16}$ molec cm^{-2}. Other areas with enhanced NO_2 columns include the cities of Toledo, Sarnia, and Cleveland. The waterways between Lake Huron and Lake Erie, one of the busiest waterways in the world, (St. Clair River and Detroit River) are also hot spots for enhanced columns of NO_2, and likely indicative of the heavy ship traffic and associated industrial activities supported by the presence of the waterway transport. Also visible from the satellite are enhanced NO_2 columns extending well out into the lakes at the ends of these waterways; Lake Erie (south of Detroit) and Lake Huron (north of Sarnia) which are likely indicative of the emissions from underway vessels, anchored vessels awaiting entry into the waterways and recreational boating activities. Considering just the NO_2 VCDs over Lake Erie, the western region of the Lake appears to be the most polluted. In contrast, the measurement site at Ridgetown can be seen to be in a relatively rural area with a study average NO_2 VCD of $\sim$2–3$\times 10^{15}$ molec cm^{-2}. The lowest VCDs in the domain are seen over Lake Erie, south of London, and in regions surrounding London to the north and west.

4.5 Comparison between VCDs and ground level concentrations of NO_2

To examine the relationship between NO_2 vertical columns and NO_2 concentrations at ground level, average NO_2 concentrations were calculated for the time periods of all VCD_{RTM} determinations. In this analysis and in the case studies to follow, we have used the NO_2 determined from the chemiluminescence instrument (Sect. 2.8) due to the continuous and higher temporal resolution of data available from this instrument compared to the active DOAS instrument. It is well known that the "NO_2" reported for these instruments may be biased high since they may contain some contribution from NO_Z species ($NO_Z = NO_y - NO_x$) due to reduction of NO_Z by the Mo convertor. However, for most of the periods of discussion to follow, we generally found good agreement between the NO_2 reported by the chemiluminescence and active DOAS instrument, apart from some early morning periods when we suspect that HONO and HNO_3 accumulated overnight may have contributed to the signal. Figure 12 shows three polar class scatter plots using the various NO_2 measures; where the NO_2 VCD_{RTM}, NO_2 number

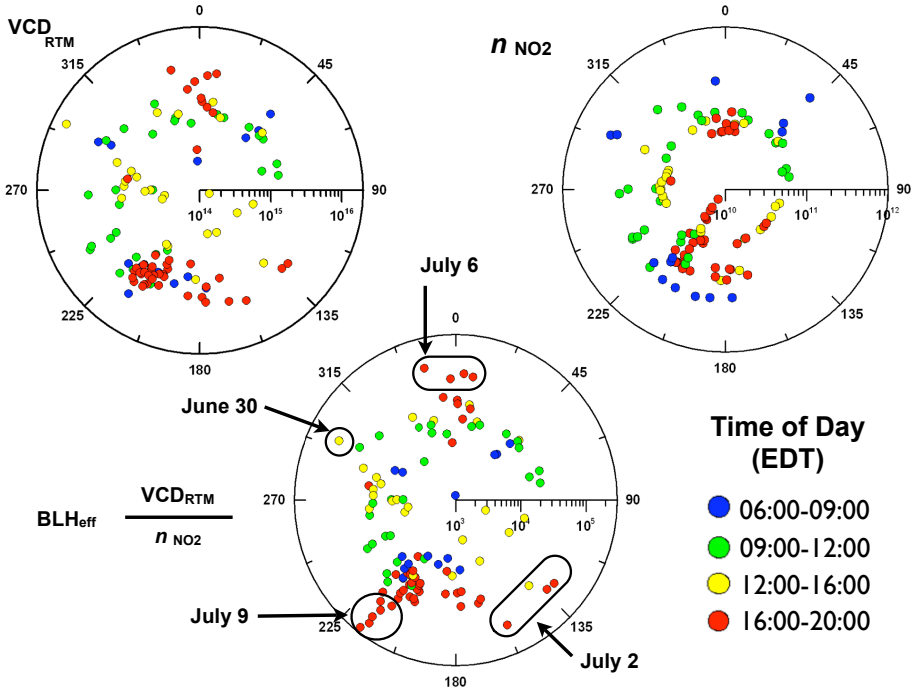

Fig. 12. Polar class scatter plot diagrams for Ridgetown. The NO_2 VCD_{RTM} (molec cm^{-2}), the NO_2 number density (molec cm^{-3}), and the BLH_{eff} (cm), are plotted on the radial axis vs. the wind direction, and are color-coded for the time of day of each measurement.

Table 3. Average VCD_{RTM}, ground NO_2, and BLH_{eff} for selected time periods at Ridgetown.

Time Period (EDT)	VCD_{RTM} ($\times 10^{15}$ molec cm^{-2})	n_{NO_2} ($\times 10^{10}$ molec cm^{-3})	BLH_{eff} (m)
06:00–09:00	2.4 ± 0.8	21.4 ± 3.2	119 ± 45
09:00–12:00	2.1 ± 0.7	10.6 ± 1.7	203 ± 77
12:00–16:00	1.5 ± 0.5	6.4 ± 1.0	201 ± 77
16:00–20:00	2.7 ± 0.9	7.1 ± 1.0	521 ± 198

density (n_{NO_2}), and the ratio VCD_{RTM}/n_{NO_2} are plotted on the radial axis respectively, as a function of the average wind direction and the time of day, color-coded into 4 binned daytime periods. The temporal behavior of the NO_2 measures within each time bin are also tabulated in Table 3, irrespective of wind direction.

Four dominant factors can contribute to the daytime temporal trends in NO_2 observed at the site: (i) temporal changes in emission rates of local NO_x sources, (ii) changes in dilution effects of boundary layer NO_2 brought about by changes in the boundary layer height, (iii) changes in the Leighton ratio, $[NO_2]/[NO]$, brought about by changes in the photolysis rate of NO_2, and (iv) changes in advection patterns. The ground-based NO_2 concentrations show a clear dependence on the time of day, both in Fig. 12 and Table 3. The highest concentrations are seen in the early morning decreasing by a factor of $\sim$3 by the afternoon. The decrease in NO_2 from early morning to afternoon is likely indicative of a combination of increased dilution in a growing boundary layer, as well as increased photoylsis of NO_2. The photolysis of NO_2 would give highest losses around solar noon (13:31 EDT at this site), and a corresponding minimum in the middle of the day. The lack of a significant minimum in the central bins of n_{NO_2} in Table 3 indicates that increased dilution in a growing boundary layer is the dominant factor that contributes to the temporal pattern seen for the NO_2 concentration. Conversely, the VCD_{RTM} shows less dependence on the time of day (Table 3 and Fig. 12), compared to the NO_2 concentration, and the temporal trend contains a minimum in the middle of the day. This is to be expected, as the column density of a pollutant in the boundary layer should be independent of dilution effects resulting from changes in the boundary layer height. The minimum VCD (1.5×10^{15} molec cm^{-2}) is observed in the bin that contains solar noon (Table 3) when NO_2 photolysis would be at its highest rate, while the highest VCD averages (2.4 and 2.7×10^{15} molec cm^{-2}) were found in the early morning and early evening periods, when the NO_2 photolysis rate is significantly less than solar noon. These observations indicate that the photolysis of NO_2 and consequent lowering of the NO_2/NO ratio likely play a more dominant role in the temporal behavior of the NO_2 VCD.

To examine the differences between NO_2 vertical columns and NO_2 concentrations measured at ground level, the following ratio was calculated:

$$\text{Ratio} = \frac{\text{VCD}_{\text{RTM}}}{n_{\text{NO}_2}} = \text{BLH}_{\text{eff}} \quad (3)$$

whereby the VCD_{RTM} and n_{NO_2} for identical time ranges were compared. In general, one would expect the NO_2 vertical column density and NO_2 concentration at ground level to be correlated with one another. If NO_2 is well mixed within a homogeneous boundary layer, and the vertical column is dominated by NO_2 within the boundary layer, then this ratio will be approximately equal to the boundary layer height. However, as we have already seen (Sect. 4.2), the boundary layer is not always well mixed, and free tropospheric NO_2 can also contribute to the vertical column of NO_2, creating a deviation of the ratio from the true boundary layer height. For these reasons, we call this ratio the effective boundary layer height, BLH_{eff}. A value of BLH_{eff} higher than the actual boundary layer height would be observed under the following conditions: (i) an elevated plume of NO_2 exists above the surface site or (ii) the column of NO_2 in the free troposphere is a significant fraction of the total tropospheric column (e.g. likely observed under conditions when the boundary layer is relatively unpolluted). Conversely, values of BLH_{eff} lower than the actual boundary layer would be observed when surface sources of NO_2 are not well mixed in the boundary layer, which could occur under conditions of relative atmospheric stability. In addition to these deviations of BLH_{eff}, we also expect that the temporal pattern of BLH_{eff} will generally follow the temporal pattern of the real boundary layer height.

The values of BLH_{eff} observed during this study ranged from 12 m (observed in early morning) to 2.54 km (observed in late afternoon). In general the BLH_{eff} increased from early morning to the end of the day (Table 3, Fig. 12), although the average values observed in the early afternoon ($\sim$200 m) are less that one would expect for continental boundary layer heights in midsummer in this region. This likely indicates that NO_2 is not homogeneously mixed in the boundary layer, as we directly observed by the aircraft measurements on 26 June (Sect. 4.2). Instructive here is to identify cases where the VCD measured by MAX-DOAS shows something different than what is measured by the more conventional surface-based point source measurement of NO_2. These cases would be indicated by the highest and lowest values of BLH_{eff}. The periods of low BLH_{eff} are somewhat trivial and are all isolated to early morning events, when a nocturnal inversion is still intact. During such periods, the NO_2 accumulated throughout the night from regional surface sources are trapped in the low inversion creating relatively high concentrations of NO_2 but only low or moderate tropospheric VCDs. More interesting are periods with high levels of BLH_{eff}, during which a ground-based measurement of NO_2 concentration would underestimate the total amount of NO_2 in the troposphere and transport of NO_2 into the region, with subsequent impacts on regional air quality. In Fig. 12, four such cases are identified as a function of the wind direction measured at ground level. The highest values of BLH_{eff} occurred on 30 June, 2, 6 and 9 July 2007.

On 30 June (between 12:00–12:40 EDT), the highest value of VCD_{RTM} determined in the study was recorded (1.25×10^{16} molec cm^{-2}) and the BLH_{eff} rose to 998 m. During this case, an elevated plume of NO_2 impacted the site from the NW that we attribute to industrial point sources in Sarnia. This case is discussed in further detail in the next section. On 2 July (between 15:00–18:00 EDT), on an otherwise cool, clear and clean day, the VCD_{RTM} increased to 5×10^{15} molec cm^{-2} and $\text{BLH}_{\text{eff}} = 991$ m with virtually no increase in the ground level concentration of NO_2. We attribute this case to impact by elevated forest fire plumes, originating in northern Ontario that moved southward, while the ground level at Ridgetown experienced a clean lake breeze inflow from the southeast. On 6 July, the BLH_{eff} had a maximum of 1.08 km early in the evening (17:00–19:00 EDT). Winds during this time were from the N–NW and the presence of elevated SO_2 indicates that the site was impacted by a mixture of industrial emissions from Sarnia, and possibly marine vessel emissions from ships on Lake Huron. The high boundary layer height would be typical of a lake breeze layer thermally modified after traveling 70 km inland (Sills et al., 2011). On 9 July late in the afternoon, the highest values of BLH_{eff} (up to 2.5 km) were seen. This case was characterized by strong winds from the SW that is characteristic for southern Ontario, evidence for strong convection and extremely high pollution levels, a classic case of a pollution episode with long-range transport of pollutants from the SW. This case will also be discussed in more detail in the next section.

4.5.1 Case studies

For the case studies that follow, the residual sum of squares (RSS), as described in the Supplemental Material, was used as an indicator of the quality of the fits between measured and modeled τ_{RTM} and VCD_{RTM} values. Values of RSS$<$0.25 were deemed to be good fits, values with 0.25$<$RSS$<$2.5 are more uncertain. Values of RSS$>$2.5 were very uncertain and were removed from the data set. These thresholds were chosen based on empirical considerations to differentiate between fits with low and high uncertainty. Values with 0.25$<$ RSS $<$2.5 are marked accordingly on Figs. 13, 15, and 16 (RSS$>$0.25) as being more uncertain, usually as the atmosphere was not behaving as per the assumption in the RTM (e.g. horizontal homogeneity). Data points with these intermediate RSS values do not necessarily represent poor results, but they indicate values that can have larger uncertainties due to limitations in the forward model, measurement errors, or temporal variations of the atmospheric properties during an elevation sequence.

Figure 13 summarizes measurements made on 30 June 2007 at Ridgetown. The synoptic flow was gentle and from the northwest in the morning period.

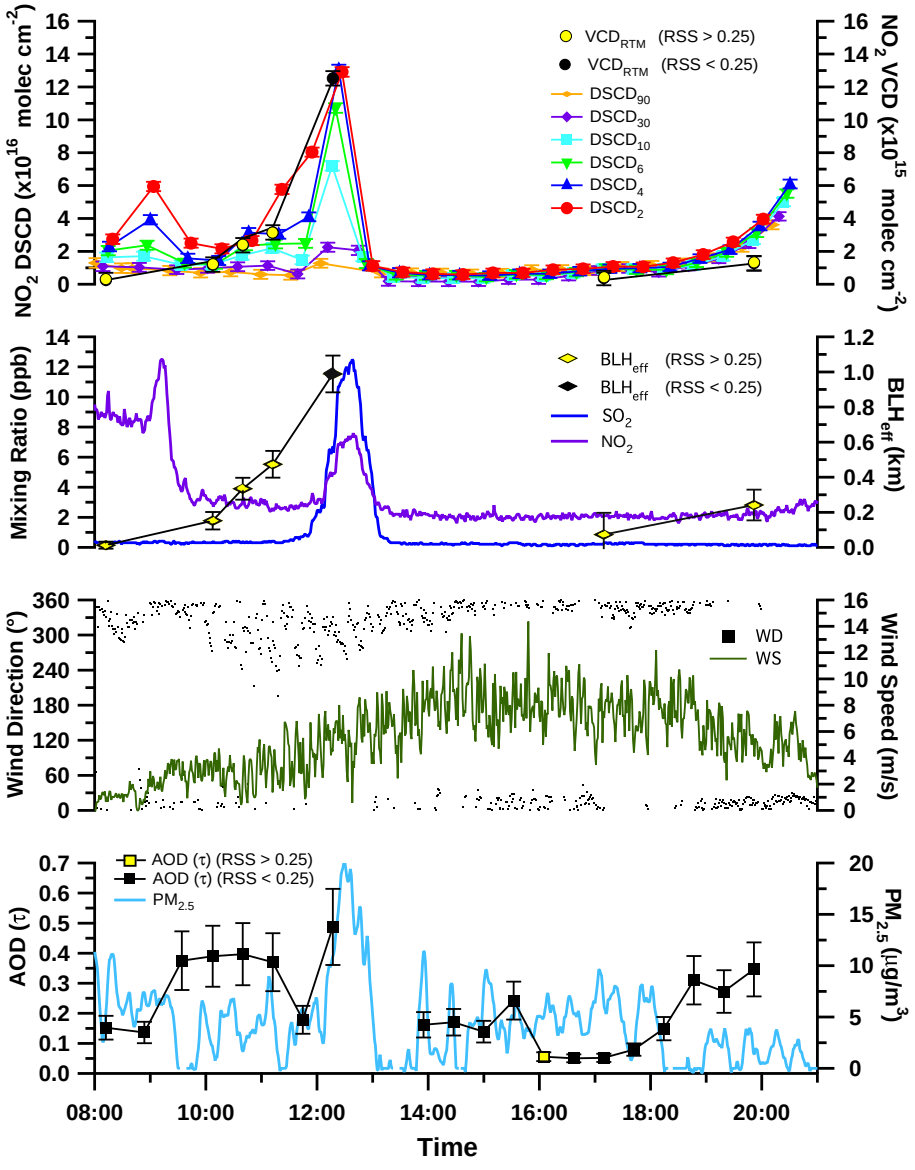

Fig. 13. Measurements at Ridgetown on 30 June 2007. NO_2 MAX-DOAS DSCDs with NO_2 VCD_{RTM} values are followed by ground level measurements of SO_2 and NO_2, BLH_{eff}, wind direction, wind speed, $PM_{2.5}$, and AOD (τ_{RTM}).

Relatively high levels of ground level NO_2 (8–12 ppb) but low levels of SO_2 were seen in the morning period 08:00–10:00 EDT. At the same time, the NO_2 VCD_{RTM} was quite low ($<1\times10^{15}$ molec cm^{-2}), and BLH_{eff} was $\leq$150 m, indicating a shallow inversion layer. Ground level NO_2 mixing ratios decreased rapidly due to the breakup of the nocturnal inversion at about 09:30 EDT and leveled off for the remainder of the morning at $\sim$2 ppb. The characteristic feature on this day was a pollution plume of $\sim$1 h duration that impacted the site between 12:00–13:00 EDT. During this short interval, daily maxima were observed for DSCDs ($\alpha = 2°$, 4°, 6°, 10°), VCD_{RTM}, τ_{RTM}, $PM_{2.5}$, SO_2, BLH_{eff} (Fig. 13), and O_3 (52 ppb, not shown). The maximum of the pollution plume coincided with the arrival of a meteorological feature that had several characteristics of a lake breeze front arriving from Lake Huron to the north. Evidence for this was an increase in the relative humidity, a slight drop in temperature, and a subtle, gradual but discernible shift in wind direction towards the north. It also coincided with arrival from the north of a thin east-west line of cumulus clouds that moved across Ridgetown between 12:00 and 13:00 EDT. The thin line of clouds provides evidence for enhanced lift along the line of this feature, typical of a lake breeze front (Sills et al., 2011). While final results from an observational analysis by Sills et al. (2011) did not specifically identify a feature with gradients that

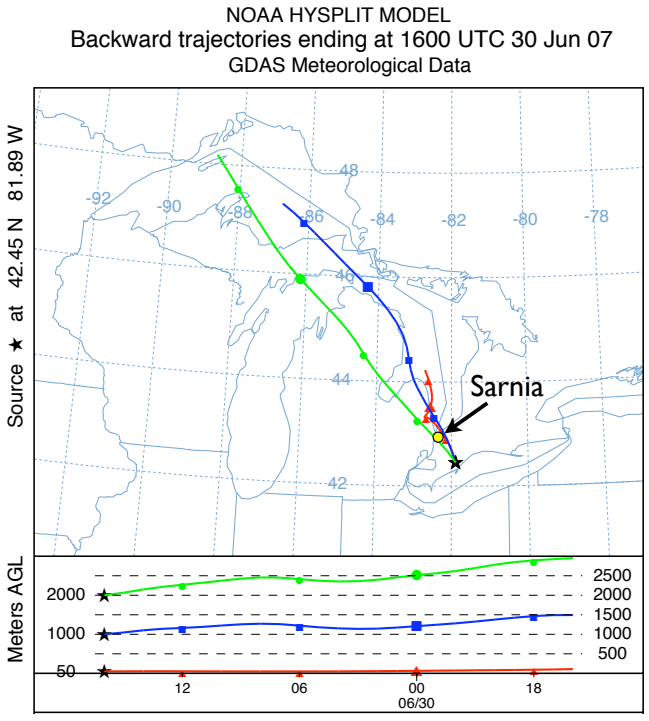

Fig. 14. HYSPLIT back trajectory for Ridgetown (starred) on 30 June 2007. Time scale in UTC.

were sharp enough to be called a lake breeze front, there is consensus that the Ridgetown site was experiencing a Lake Huron lake breeze by 14:00 and that this meteorological feature with enhanced lift preceded the arrival of the lake breeze. The results from the MAX-DOAS measurements are particularly informative at this time. In particular, while the DSCDs of NO_2 increased at all elevation angles, the DSCD with $\alpha = 4°$, $DSCD_4$, was marginally higher than the $DSCD_2$ (though the difference is not statistically significant). This is an observation that rarely occurs, even under high aerosol conditions when the absorption length through the lower atmosphere becomes similar at all elevation angles, making all DSCDs similar. This result can be contrasted to the result early in the morning when the nocturnal boundary layer was still intact. During that early morning period, we observed the typical situation in which $DSCD_2 > DSCD_4 > DSCD_6 > DSCD_{10} > DSCD_{30}$, commonly seen when a polluted layer exists at the surface, where larger DSCDs are observed at lower elevation angles due to the larger effective path length of scattered light through the polluted layer (Hönninger et al., 2004). In addition, it can be observed during the time just preceeding the pollution plume peak that the $DSCD_2$ and $DSCD_4$ increase before the other DSCDs and well before the ground level in-situ observations of NO_2 and SO_2 show any detectable increase. This points towards a temporal effect whereby an inhomogeneous plume moves into the complex viewing geometry of the MAX-DOAS. Both effects strongly suggest that the polluted layer was elevated from the surface, or had higher concentrations above the surface than at ground level (Hönninger et al., 2004). Other evidence that the pollution plume was elevated was the rapid increase in the value of BLH_{eff}. Despite the presence of an elevated plume, increases in SO_2, NO_2, and NO_x were still seen at ground level during this time period of the plume, which coincided with the arrival of the lake breeze. This suggests that the elevated plume was mixed partially to the surface (but not homogeneously) through a process similar to fumigation, where smokestack effluent brought inland in stable stratified marine air is mixed to the surface when it intersects the convective mixed layer at the lake breeze front (Lyons and Cole, 1973; Sills et al., 2011).

Wind Directions on 30 June 2007 were N–NW (Fig. 13) and the pollutant plume between 12:00–13:00 EDT may be traced back to the region of Sarnia, Ontario ∼70 km away, using the NOAA HYSPLIT (Draxler and Rolph, 2011) back trajectory analysis (Fig. 14). Many anthropogenic sources with elevated stack emissions are located close to the Lake Huron shoreline close to Sarnia, including petrochemical refineries, other chemical industries, and a major coal fired electric generation facility in Lambton, Ontario. The excess SO_2/NO_x ratio (mole mole^{-1}) in the pollution plume at ground level during the pollution event was calculated to be 2.21 ± 0.08 mole mole^{-1}. This can be compared to emissions from the largest point sources within a 5 km radius of Sarnia that contain stacks. According to the National Pollutant Release Inventory (EC, 2011), the total emissions of SO_2 and NO_x from the top 10 point sources in Sarnia are 23.9 kt yr^{-1} and 5.82 kt yr^{-1} respectively, with a SO_2/NO_x ratio of 2.95 mole mole^{-1}, dominated by refinery emissions. The corresponding emissions of SO_2 and NO_x from the stack of the Lambton coal-fired electric utility (∼16 km south of the major refineries in Sarnia) are 6.19 kt yr^{-1} and 3.96 kt yr^{-1}, with a SO_2/NO_x ratio of 1.10 mole mole^{-1}. Although we cannot identify a single source from this, the evidence suggests that the plume impacting the site during this period was from either one or several elevated fuel combustion sources that fumigated to the surface as the lake breeze front passed Ridgetown. After this time, the winds at the site continued to shift towards a more northerly direction and the site experienced a clean lake breeze from Lake Huron for the rest of the afternoon, devoid of surface or elevated pollution sources of NO_2. While evidence points to the fact that the plume was elevated, an explanation is still required for the large increase in the VCD and simultaneous arrival with the lake breeze. A lake breeze front is known to be a narrow convergence zone with enhanced lift that can transport pollutants upward (Sills et al., 2011). The front can also result in a region of spatial stagnation, with respect to the inflow layer, if the speed of the front moves slower than the inflow layer. The dynamics of both lift, and recirculation that exist at the front (Lyons and Cole, 1973; Sills et al., 2011) can thus result in a higher concentration of pollutants at the leading

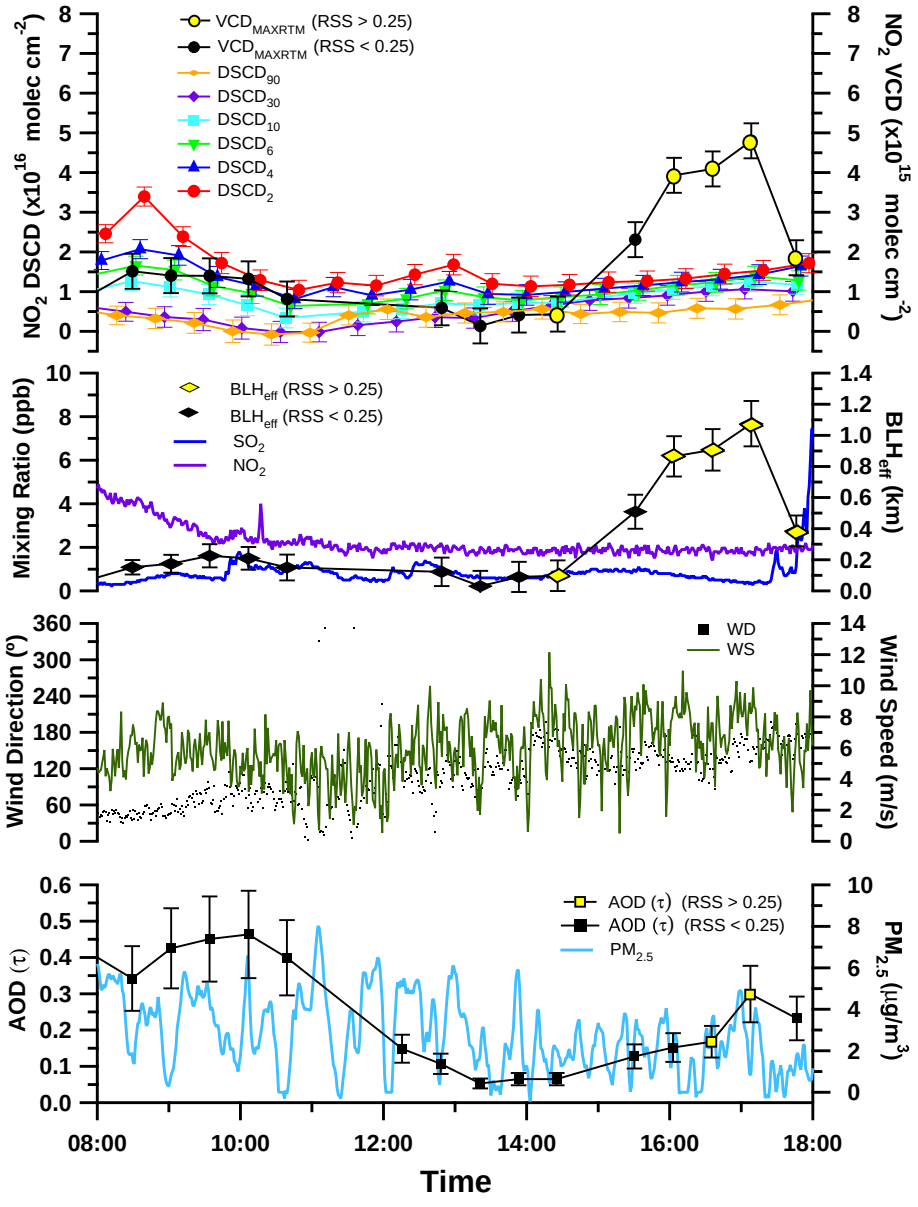

Fig. 15. Measurements at Ridgetown on 2 July 2007. NO_2 MAX-DOAS DSCDs with NO_2 VCD_{RTM} values are followed by ground level measurements of SO_2 and NO_2, BLH_{eff}, wind direction, wind speed, $PM_{2.5}$, and AOD (τ_{RTM}).

edge of a lake breeze, that is still not completely understood. Our result presents evidence (perhaps for the first time) that these dynamics can lead to an overall increase in not only the concentration of pollutants, but also the vertical column of pollutants as well. This is the first demonstration of such an effect using MAX-DOAS, to the best of our knowledge.

Figure 15 summarizes measurements made on 2 July 2007. The area was under the influence of a regional high pressure system on this day with light winds, sunshine, cool temperatures (<21 °C) and low deformation lake breeze conditions (Sills et al., 2011). Ground level pollution (SO_2, NO_2, $PM_{2.5}$, O_3) was low throughout most of the day, as was O_3 (<35 ppb, not shown). The MAX-DOAS measurements indicated a clean troposphere with VCDs $<2\times10^{15}$ molec cm^{-2} and BLH_{eff} <200 m prior to 15:00 EDT, indicating either a shallow or inhomogeneously mixed boundary layer with NO_2 confined to the surface. By late morning and throughout the afternoon, the site was experiencing a moderate lake breeze from the S–SE (Lake Erie) although satellite imagery indicates that upper air movement was from the W–NW. After 15:00 EDT, the VCDs of NO_2 showed an appreciable increase from $\sim5\times10^{14}$ molec cm^{-2} up to 5×10^{15} molec cm^{-2}, while the BLH_{eff} increased from less than 100 m to greater than 1 km.

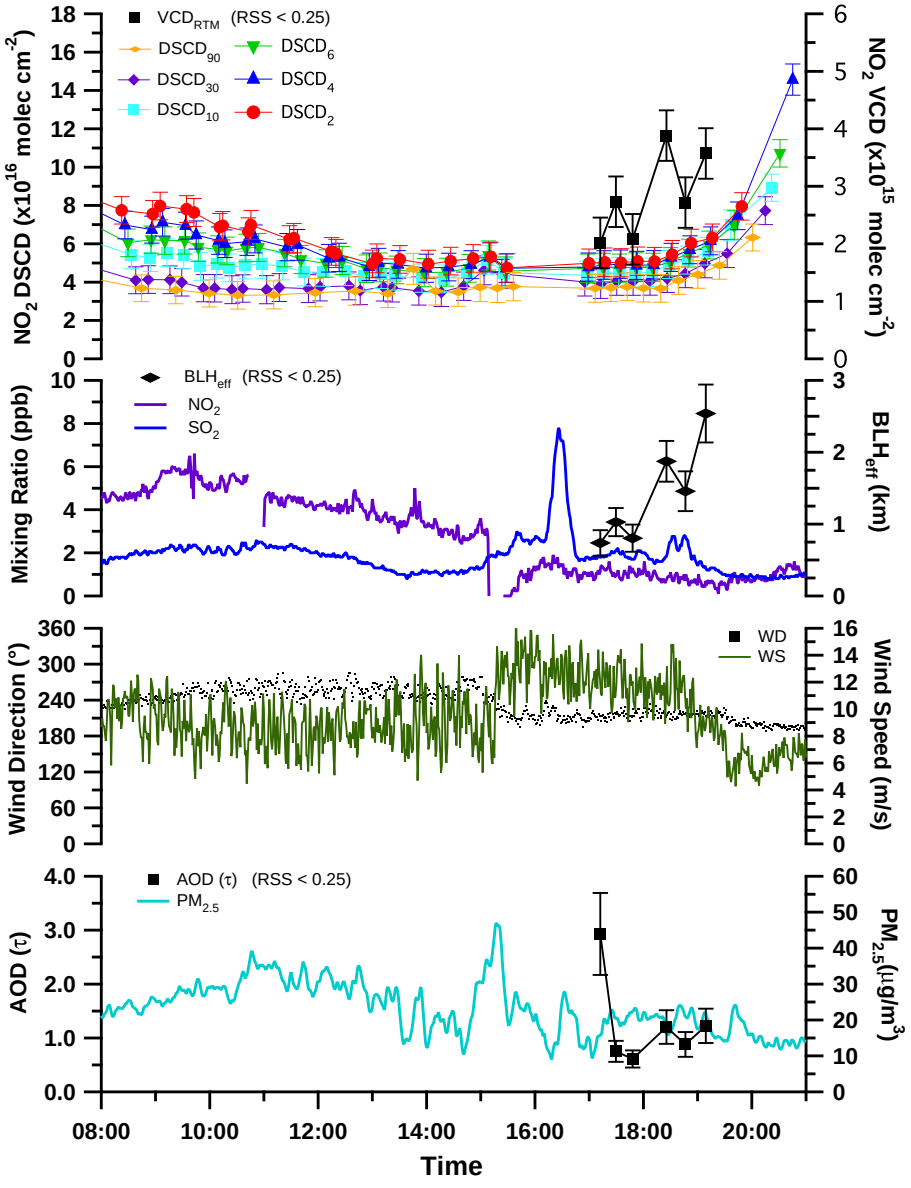

Fig. 16. Measurements at Ridgetown on 9 July 2007. NO_2 MAX-DOAS DSCDs with NO_2 VCD_{RTM} values are followed by ground level measurements of SO_2 and NO_2, BLH_{eff}, wind direction, wind speed, $PM_{2.5}$, and AOD (τ_{RTM}).

A close examination showed that the ground level mixing ratio of NO_2 remained unchanged at ~2 ppb throughout this period, indicating that the increase in vertical column of NO_2 was not due to a surface source of NO_2. Unlike the elevated plume seen on 30 June, in this case the DSCDs at lower elevation angles ($DSCD_2$, $DSCD_4$) did not show any appreciable increase. Further examination indicates that the increase in the VCD is being largely driven by the increase in $DSCD_{30}$ (VCD_{30}). In a qualitative sense, this indicates that the elevated NO_2 must be at very high elevation from the surface, much higher than seen on 30 June. Indeed, elevated forest fire plumes were reported in Southern Ontario on this day. They were clearly visible as brown streaks moving south in the sky at high altitude, likely in the upper free troposphere. An analysis of satellite imagery and fire occurrences using the Canadian Wildland Fire Information System (http://cwfis.cfs.nrcan.gc.ca/en_CA/index) for several days prior and following this date indicated the most likely source to be an intense line of boreal forest fires that had started on or about 28 June close to the Saskatchewan/Northwest Territories border approximately 2500 km northwest of the site. Although the aerosol optical depth was higher in the morning ($\tau_{RTM} = 0.4$), likely due to anthropogenic aerosol pollution from urban areas to the northeast, the τ_{RTM} also increased marginally ($\Delta\tau_{RTM} = +0.2$) during the biomass burning plume event, while $PM_{2.5}$ remained

unchanged. This indicated that only a small amount of aerosol was associated with the plume, perhaps due to sedimentation during the ∼2 day transport time. Despite this, particle-based receptor modeling of aerosol time of flight mass spectrometry data identified the beginning of an event of aged biomass burning particles at Harrow, ON late in the day or early morning on 2/3 July (McGuire et al., 2011). It is acknowledged that the determination of τ using the method outlined here is highly uncertain in a case such as this and would likely benefit from a two level retrieval system, as there are likely two distinct layers of NO_2 and aerosols. As O_4 has a scale height of ∼4 km in the atmosphere, the use of changes in the O_4 absorption to predict the presence of aerosols will be much less sensitive with aerosol layers in the upper troposphere. Therefore, the value of τ_{RTM} will likely underestimate the true tropospheric AOD in such cases. This could be the situation for the current case study. The VCD_{RTM} could also be uncertain due to multiple scattering events in a mixed aerosol-NO_2 plume in the upper troposphere, however it is unlikely to be as sensitive as the AOD, and the prediction of the direction of bias in NO_2 VCD is uncertain without further 2 level radiative transfer modeling. Despite this, the case illustrates a situation where transport of pollution through the region at high altitude was detected by MAX-DOAS, which would be virtually undetected at ground level using standard air quality instrumentation.

Figure 16 summarizes measurements made on 9 July 2007. This day was characterized by warm temperatures (33 °C maximum), hazy conditions with strong W–SW synoptic flow, high deformation lake breeze circulations, and enhanced turbulence (Sills et al., 2011). High pressure existed south east of the Great Lakes, a typical situation for the transport of ozone and aerosol precursors into southern Ontario from the SW (MOE, 2011). Indeed, aerosols were abundant with $PM_{2.5}$ levels in the range of 10–50 µg m^{-3}, and τ_{RTM}∼1.0±0.2 in late afternoon, apart from a single value of 2.8 at 17:00 EDT. Ozone (not shown) also recorded a maximum of 87 ppb, a few minutes prior to the passage of a lake breeze front. Due to the cumulus clouds in the vicinity for much of the day, VCD_{RTM} could not be determined until after 17:00 EDT. Winds that were from the W–SW (260°) at 9 m s^{-1}, switched to S–SW (215°) at 13 m s^{-1} with gusts up to 17 m s^{-1} at 15:10 EDT, indicating the passage of the lake breeze front (Lake Erie), and accompanied with an increase in relative humidity, spikes in $PM_{2.5}$, CO and O_3 (not shown), and a drop in NO_2. Between 17:00 and 19:15 EDT, conditions were hazy but cloud-free such that estimates of VCD_{RTM} were determinable. The NO_2 was relatively low, between 0.5 and 1.5 ppb, while VCDs ranged from 2–4×10^{15} molec cm^{-2}, and BLH_{eff} increased from 800 m to 2600 m at 17:10 EDT. The DSCDs do not give any indication of an elevated plume, and a measure of the true boundary layer height was not available at Ridgetown on this day. However, the potential temperature profile measured by sonde release at White Lake, Michigan, just northwest of Detroit (Station DTX, #72632), indicated a subsidence inversion at 1.90 km at 20:00 EDT (UWYO, 2010), that was comparable to the average BLH_{eff} measured between 19:20 and 18:20 EDT (1.93 km). Thus, on this particular day, when strong wind speeds and strong convection would support a well mixed boundary layer, the value of BLH_{eff} was comparable to the true boundary layer height measured in a continental region close to the site. This provides an opportunity to further validate our VCD_{RTM} determinations during this time period. Between 18:00 and 19:00, the average VCD_{RTM} was 3.4±0.5×10^{15} molec cm^{-2}. The tropospheric VCD of NO_2 estimated from the average NO_2 mixing ratio (0.8 ppb) in a homogeneous boundary layer of 1.9 km is 3.8 × 10^{15} molec cm^{-2}. These numbers agree reasonably well. This case, where the boundary layer is relatively homogeneous and well mixed, is one of the few situations during the study where we expect this to be true. In such a case, the mixing ratio of NO_2 measured at ground level is quite low, and may not indicate the total amount of NO_2 being transported into the region in the deep boundary layer. To estimate the total transport of tropospheric NO_2 across a boundary tangential to the wind direction during this pollution event, the flux of tropospheric NO_2 perpendicular to the wind direction, F_{NO_2} (molec s^{-1}), could be calculated according the following equation:

$$F_{NO_2} = VCD_{NO_2} \times L \times u_{trop} \quad (4)$$

where L is the length of a border, and u_{trop} is the average flow rate of the troposphere. Using the wind speed at 10 m height (12 m s^{-1} in late afternoon) as a lower limit of the flow rate in the lower troposphere, and the average VCD_{RTM} in the later afternoon period (3.4 × 10^{15} molec cm^{-2}), we conservatively estimate the line flux (F_{NO_2}/L) of NO_2 through the region to be greater than 4.1 × 10^{18} molec cm^{-1} s^{-1}, or 112 kg NO_2 km^{-1} h^{-1}, during the pollution event. This may be a useful parameter to compare with model estimates of transport fluxes where they exist.

5 Conclusions

We outline an original method for the determination of aerosol optical depths and vertical column densities of NO_2 using a combination of MAX-DOAS measurement of NO_2 and O_4, radiative transfer, and inversion modeling. The aerosol optical depths ($\lambda = 360$ nm) determined with this method were compared to other measures of aerosol optical depth regionally available (OMI, MODIS, AERONET) with some qualitative agreement, although differences in the wavelengths used and spatial locations prevented a more direct comparison of these measures. A direct comparison between τ_{RTM} and $PM_{2.5}$ measured at the site gave a very low level of correlation, while a direct comparison between the calculated aerosol extinction coefficient (τ_{RTM}/H_{aer}) and

$PM_{2.5}$ gave a much higher correlation and a mass specific extinction coefficient of $16 \pm 1\,m^2\,g^{-1}$. While H_{aer} is not expected to be equivalent to the true boundary layer height, the improved correlation emphasizes the importance of taking into account boundary layer heights in any attempts to link aerosol optical depths determined by satellite, for example, with human exposure of aerosols at ground level.

The tropospheric VCDs of NO_2 derived this way, VCD_{RTM}, were compared to tropospheric VCDs compiled through vertical measurements of NO_2 close to the site, VCD_{COMP}. On average, VCD_{RTM} was only 2 % lower than VCD_{COMP}; the difference is not statistically significant. This serves as a validation for the method outlined here for determining NO_2 VCDs. Intercomparison of satellite instrument derived VCDs with a limited number of comparison points from OMI ($N = 8$) and SCIAMACHY ($N = 1$) indicate that the satellite derived measures were ∼50% higher than VCD_{RTM} with a mean bias of $+0.9\times10^{15}$ molec cm^{-2} for OMI (statistically significant), and $+0.5\times10^{15}$ molecules cm^{-2} for SCIAMACHY (not statistically significant). It should be taken in context that the apparently large relative overprediction by the satellites retrievals (+50%) could easily be due to a small constant bias coupled with the overall relatively small tropospheric VCDs of NO_2 that were experienced in this rural region. The relevance of the result to more polluted regions with higher VCDs should be verified.

Previous literature has reported the opposite, namely that satellite derived measures of VCD are on average smaller than VCDs found via MAX-DOAS. The root cause for these differences is probably the different nature of the measurement sites; rural in this study compared to more urban in previous reports, or the overall values of the NO_2 VCDs, which were much lower in this study compared to previous reports. Typically, VCDs derived from MAX-DOAS in previous comparisons with satellite measures of NO_2 have used a geometrical approximation to estimate the air mass factor and VCD, similar to the VCD_{GEO} values reported here. Our VCD_{GEO} values were marginally lower than our VCD_{RTM} values, but only for a small subset of comparisons with a stringent criteria, namely that the VCDs determined using a geometric approximation with elevation angles of 10° and 30° agree to within 15 %. The methodology we outlined here to determine VCD_{RTM} is not as stringent, and has allowed us to determine VCDs over a much wider range of aerosol conditions than would otherwise be possible using just the geometric approximation.

We define the ratio of the tropospheric VCD and ground level concentration of NO_2 to be the effective boundary layer height, BLH_{eff}. The diurnal pattern of BLH_{eff} generally follows the expected pattern for the boundary layer height during the day; although we find values of BLH_{eff} are generally lower than expected for continental boundary layer heights in late afternoon, likely due to surface sources in a boundary layer that is not well mixed. We illustrate exceptions to this in three case studies. In two of the cases, we show high values of BLH_{eff} are due to elevated plumes of NO_2, one from elevated stack emissions from industry, and one from biomass burning plumes that were transported through the region. In the third case, we found that BLH_{eff} was very high (∼2 km) and similar to the measured continental boundary layer height just northwest of the study region, likely as a result of instability in the atmosphere that promoted convection and efficient mixing throughout the boundary layer. The variations of BLH_{eff} with time of day and conditions, should be considered in attempts to determine ground level concentrations of NO_2 from satellite derived measures, or in attempts to validate satellite measurements through use of ground-based measurements.

The case studies examined here also provide some interesting examples of transport of pollutants in this region and the interaction with lake breezes that exist due to the presence of the surrounding lakes. In our first case study, we present an example of suspected fumigation of elevated industrial pollutants brought to the surface at a lake breeze, and an increase in the total NO_2 VCD at the lake breeze. Our last case study occurred during a regional smog event with transport of ozone and aerosol precursors from the southwest. Although ground level concentrations of NO_2 were quite low during this event (<1.5 ppb), the column amount of NO_2 was more substantial than otherwise suspected due to a deep and well mixed boundary layer. We have estimated the line flux of NO_2, at this time, to be greater than 112 kg $NO_2\,km^{-1}\,h^{-1}$. Multiplication of the line flux by the width of a boundary line perpendicular to the prevailing wind direction would give the total mass transport of tropospheric NO_2 across the boundary line, during the regional pollution event.

Supplement related to this article is available online at: http://www.atmos-chem-phys.net/11/12475/2011/acp-11-12475-2011-supplement.pdf.

Acknowledgements. The authors wish to acknowledge funding from NSERC and from a grant provided by the Ontario Ministry of the Environment. LIDAR information was provided by B. Firanski and K. Strawbridge, Environment Canada. OMI data was obtained and processed through joint research between the Netherlands (NIVR/KNMI), Finland (FMI), and the US (NASA) in the Earth Observing System (EOS) Aura Mission, J. P. Veefkind (KNMI) and J. F. Gleason (NASA), Principal Investigators. For AERONET data (Egbert), technical support was provided by I. Abboud of Environment Canada and J. Freemantle of the Universite de Sherbrooke, while N. O'Neill and B. McArthur were the scientific principal investigators. For AERONET data (Kellogg), P. Robertson was the principal investigator. Thanks to the NOAA Air Resources Laboratory (ARL) for the provision of the HYSPLIT model. Special thanks to D. Sills for his insight with respect to the meteorology at Ridgetown, T. Deutschmann, the developer of the McArtim RTM, E. Celarier, I. Levy, A. Freedman, T. Onasch, and P. Massoli for helpful discussions, and C. Weldon

and P. Wojtal for proofreading the manuscript. Finally, thanks to the anonymous referees for their helpful comments and suggestions.

Edited by: J. Abbatt

References

Alicke, B., Geyer, A., Hofzumahaus, A., Holland, F., Konrad, S., Patz, H. W., Schafer, J., Stutz, J., Volz-Thomas, A., and Platt, U.: OH formation by HONO photolysis during the BERLIOZ experiment, J. Geophys. Res.-Atmos., 108, 8247, doi:10.1029/2001JD000579, 2003.

Beirle, S., Kühl, S., Puķīte, J., and Wagner, T.: Retrieval of tropospheric column densities of NO_2 from combined SCIAMACHY nadir/limb measurements, Atmos. Meas. Tech., 3, 283–299, doi:10.5194/amt-3-283-2010,1 2010.

Blond, N., Boersma, K. F., Eskes, H. J., van der A, R. J., Roozendael, M. V., Smedt, I. D., Bergametti, G., and Vautard, R.: Intercomparison of SCIAMACHY nitrogen dioxide observations, in situ measurements and air quality modeling results over Western Europe, J. Geophys. Res.-Atmos., 112, D10311, doi:10.1029/2006JD007277, 2007.

Boersma, K. F., Bucsela, E. J., Brinksma, E. J., and Gleason, J. F.: NO_2, OMI-EOS Algorithm, Theoretical Basis Document: Trace Gas Algorithms: NO_2, 12–35, 2001.

Bogumil, K., Orphal, J., Homann, T., Voigt, S., Spietz, P., Fleischmann, O. C., Vogel, A., Hartmann, M., Kromminga, H., Bovensmann, H., Frerick, J., and Burrows, J. P.: Measurements of molecular absorption spectra with the SCIAMACHY preflight model: instrument characterization and reference data for atmospheric remote-sensing in the 230–2380 nm region, J. Photoch. Photobio. A, 157, 167–184, 2003.

Bovensmann, H., Burrows, J. P., Buchwitz, M., Frerick, J., Noel, S., Rozanov, V. V., Chance, K. V., and Goede, A. P. H.: SCIAMACHY: Mission objectives and measurement modes, J. Atmos. Sci., 56, 127–150, 1999.

Brinksma, E. J., Pinardi, G., Volten, H., Braak, R., Richter, A., Schoenhardt, A., van Roozendael, M., Fayt, C., Hermans, C., Dirksen, R. J., Vlemmix, T., Berkhout, A. J. C., Swart, D. P. J., Oetjen, H., Wittrock, F., Wagner, T., Ibrahim, O. W., de Leeuw, G., Moerman, M., Curier, R. L., Celarier, E. A., Cede, A., Knap, W. H., Veefkind, J. P., Eskes, H. J., Allaart, M., Rothe, R., Piters, A. J. M., and Levelt, P. F.: The 2005 and 2006 DANDELIONS NO_2 and aerosol intercomparison campaigns, J. Geophys. Res.-Atmos., 113, D16S46, doi:10.1029/2007JD008808, 2008.

Bucsela, E., Celarier, E., Wenig, M., Gleason, J., Veefkind, J., Boersma, K. F., and Brinksma, E.: Algorithm for NO_2 vertical column retrieval from the Ozone Monitoring Instrument, IEEE T. Geosci. Remote, 44, 1245–1258, 2006.

Burrows, J. P., Richter, A., Dehn, A., Deters, B., Himmelmann, S., and Orphal, J.: Atmospheric remote-sensing reference data from GOME 2. Temperature-dependent absorption cross sections of O_3 in the 231–794 nm range, J. Quant. Spectrosc. Ra., 61, 509–517, 1999.

Celarier, E. A., Brinksma, E. J., Gleason, J. F., Veefkind, J. P., Cede, A., Herman, J. R., Ionov, D., Goutail, F., Pommereau, J. P., Lambert, J. C., Roozendael, M. V., Pinardi, G., Wittrock, F., Schoenhardt, A., Richter, A., Ibrahim, O. W., Wagner, T., Bojkov, B., Mount, G., Spinei, E., Chen, C. M., Pongetti, T. J., Sander, S. P., Bucsela, E. J., Wenig, M. O., Swart, D. P. J., Volten, H., Kroon, M., and Levelt, P. F.: Validation of ozone monitoring instrument nitrogen dioxide columns, J. Geophys. Res.-Atmos., 113, D15S15, doi:10.1029/2007JD008908, 2008.

Chance, K. V. and Spurr, R. J. D.: Ring effect studies: Rayleigh scattering, including molecular parameters for rotational Raman scattering, and the Fraunhofer spectrum, Appl. Optics, 36, 5224–5230, 1997.

Chen, D., Zhou, B., Beirle, S., Chen, L. M., and Wagner, T.: Tropospheric NO_2 column densities deduced from zenith-sky DOAS measurements in Shanghai, China, and their application to satellite validation, Atmos. Chem. Phys., 9, 3641–3662, doi:10.5194/acp-9-3641-2009, 2009.

Chu, D. A., Kaufman, Y. J., Zibordi, G., Chern, J. D., Mao, J., Li, C. C., and Holben, B. N.: Global monitoring of air pollution over land from the Earth Observing System-Terra Moderate Resolution Imaging Spectroradiometer (MODIS), J. Geophys. Res.-Atmos., 108, 4661, doi:10.1029/2002JD003179, 2003.

Clémer, K., Van Roozendael, M., Fayt, C., Hendrick, F., Hermans, C., Pinardi, G., Spurr, R., Wang, P., and De Maziére, M.: Multiple wavelength retrieval of tropospheric aerosol optical properties from MAXDOAS measurements in Beijing, Atmos. Meas. Tech., 3, 863–878, doi:10.5194/amt-3-863-2010, 2010.

Dentener, F. J. and Crutzen, P. J.: Reaction of N_2O_5 on Tropospheric Aerosols – Impact on the Global Distributions of NO_x, O_3, and OH, J. Geophys. Res.-Atmos., 98, 7149–7163, 1993.

Deutschmann, T., Beirle, S., Frieß, U., Grzegorski, M., Kern, C., Kritten, L., Platt, U., Prados-Román, C., Puķīte, J., Wagner, T., Werner, B., and Pfeilsticker, K.: The Monte carlo Atmospheric radiative transfer model McArtim: Introduction and validation of Jacobians and 3-D features, J. Quant. Spectrosc. Ra., 112, 1119–1137, 2011.

Draxler, R. R. and Rolph, G. D.:HYbrid Single-Particle Lagrangian Integrated Trajectory Model, available online at: http://ready.arl.noaa.gov/HYSPLIT.php, last access: 25 November 2011, 2011.

Dubovik, O. and King, M. D.: A flexible inversion algorithm for retrieval of aerosol optical properties from Sun and sky radiance measurements, J. Geophys. Res.-Atmos., 105, 20673–20696, 2000.

EC: Environment Canada, National Pollutant Release Inventory, available online at: http://www.ec.gc.ca/inrp-npri/default.asp?lang=En&n=4A577BB9-1, 15 March 2011, 2011.

Engel-Cox, J. A., Holloman, C. H., Coutant, B. W., and Hoff, R. M.: Qualitative and quantitative evaluation of MODIS satellite sensor data for regional and urban scale air quality, Atmos. Environ., 38, 2495–2509, 2004.

Engel-Cox, J. A., Hoff, R. M., Rogers, R., Dimmick, F., Rush, A. C., Szykman, J. J., Al-Saadi, J., Chu, D. A., and Zell, E. R.: Integrating lidar and satellite optical depth with ambient monitoring for 3-dimensional particulate characterization, Atmos. Environ., 40, 8056–8067, 2006.

Fayt, C. and Roozendael, M. V.: WinDOAS 2.1 – 2001, available online at: http://bro.aeronomie.be/WinDOAS-SUM-210b.pdf, 15 March 2011, 2011.

Finlayson-Pitts, B. J. and Pitts, J. N.: Chemistry of the Upper and Lower Atmosphere, Academic Press, San Diego, California, USA, 5–6, 1999.

Frieß, U., Monks, P. S., Remedios, J. J., Rozanov, A., Sinreich, R., Wagner, T., and Platt, U.: MAX-DOAS O_4 measurements: A

new technique to derive information on atmospheric aerosols: 2. Modeling studies, J. Geophys. Res.-Atmos., 111, D14203, doi:10.1029/2005JD006618, 2006.

Grainger, J. F. and Ring, J.: Anomalous Fraunhofer Line Profiles, Nature, 193, 762, 1962.

Greenblatt, G. D., Orlando, J. J., Burkholder, J. B., and Ravishankara, A. R.: Absorption-Measurements of Oxygen between 330 nm and 1140 nm, J. Geophys. Res.-Atmos., 95, 18577–18582, 1990.

Gupta, P. and Christopher, S. A.: Seven year particulate matter air quality assessment from surface and satellite measurements, Atmos. Chem. Phys., 8, 3311–3324, doi:10.5194/acp-8-3311-2008, 2008.

Harder, J. W. and Brault, J. W.: Atmospheric measurements of water vapor in the 442-nm region, J. Geophys. Res.-Atmos., 102, 6245–6252, 1997.

Hastie, D. R., Narayan, J., Schiller, C., Niki, H., Shepson, P. B., Sills, D. M. L., Taylor, P. A., Moroz, W. J., Drummond, J. W., Reid, N., Taylor, R., Roussel, P. B., and Melo, O. T.: Observational evidence for the impact of the lake breeze circulation on ozone concentrations in Southern Ontario, Atmos. Environ., 33, 323–335, 1999.

Hayden, K., Sills, D., Brook, J., Li, S., Makar, P., Markovic, M., Liu, P., Anlauf, K., O'Brien, J., Lin, Q., and McLaren, R.: Aircraft study of the impact of lake-breeze circulations on trace gases and particles during BAQS-Met 2007, Atmos. Chem. Phys., 11, 10173–10192, doi:10.5194/acp-11-10173-2011, 2011.

Heckel, A., Richter, A., Tarsu, T., Wittrock, F., Hak, C., Pundt, I., Junkermann, W., and Burrows, J. P.: MAX-DOAS measurements of formaldehyde in the Po-Valley, Atmos. Chem. Phys., 5, 909–918, doi:10.5194/acp-5-909-2005, 2005.

Heland, J., Schlager, H., Richter, A., and Burrows, J. P.: First comparison of tropospheric NO_2 column densities retrieved from GOME measurements and in situ aircraft profile measurements, Geophy. Res. Lett., 29, 1983, doi:10.1029/2002GL015528, 2002.

Hendrick, F., Van Roozendael, M., Kylling, A., Petritoli, A., Rozanov, A., Sanghavi, S., Schofield, R., von Friedeburg, C., Wagner, T., Wittrock, F., Fonteyn, D., and De Maziére, M.: Intercomparison exercise between different radiative transfer models used for the interpretation of ground-based zenith-sky and multi-axis DOAS observations, Atmos. Chem. Phys., 6, 93–108, doi:10.5194/acp-6-93-2006, 2006.

Holben, B. N., Eck, T. F., Slutsker, I., Tanre, D., Buis, J. P., Setzer, A., Vermote, E., Reagan, J. A., Kaufman, Y. J., Nakajima, T., Lavenu, F., Jankowiak, I., and Smirnov, A.: AERONET – A federated instrument network and data archive for aerosol characterization, Remote Sens. Environ., 66, 1–16, 1998.

Holben, B. N., Tanre, D., Smirnov, A., Eck, T. F., Slutsker, I., Abuhassan, N., Newcomb, W. W., Schafer, J. S., Chatenet, B., Lavenu, F., Kaufman, Y. J., Castle, J. V., Setzer, A., Markham, B., Clark, D., Frouin, R., Halthore, R., Karneli, A., O'Neill, N. T., Pietras, C., Pinker, R. T., Voss, K., and Zibordi, G.: An emerging ground-based aerosol climatology: Aerosol optical depth from AERONET, J. Geophys. Res.-Atmos., 106, 12067–12097, 2001.

Hönninger, G., von Friedeburg, C., and Platt, U.: Multi axis differential optical absorption spectroscopy (MAX-DOAS), Atmos. Chem. Phys., 4, 231–254, doi:10.5194/acp-4-231-2004, 2004.

Irie, H., Kanaya, Y., Akimoto, H., Iwabuchi, H., Shimizu, A., and Aoki, K.: First retrieval of tropospheric aerosol profiles using MAX-DOAS and comparison with lidar and sky radiometer measurements, Atmos. Chem. Phys., 8, 341–350, doi:10.5194/acp-8-341-2008, 2008.

Irie, H., Kanaya, Y., Akimoto, H., Iwabuchi, H., Shimizu, A., and Aoki, K.: Dual-wavelength aerosol vertical profile measurements by MAX-DOAS at Tsukuba, Japan, Atmos. Chem. Phys., 9, 2741–2749, doi:10.5194/acp-9-2741-2009, 2009.

Jacob, D. J.: Introduction to Atmospheric Chemistry, Princeton University Press, Princeton N.J., 1999.

Kacenelenbogen, M., Léon, J.-F., Chiapello, I., and Tanré, D.: Characterization of aerosol pollution events in France using ground-based and POLDER-2 satellite data, Atmos. Chem. Phys., 6, 4843–4849, doi:10.5194/acp-6-4843-2006, 2006.

Koelemeijer, R. B. A., Homan, C. D., and Matthijsen, J.: Comparison of spatial and temporal variations of aerosol optical thickness and particulate matter over Europe, Atmos. Environ., 40, 5304–5315, 2006.

Kraus, S.: DOASIS, A Framework Design for DOAS, Ph.D. thesis, University of Heidelberg, Germany, 2006.

Kurucz, R. L., Furenlid, I. J., and Testerman, L.: Solar Flux Atlas from 296 to 1300 nm, National Solar Observatory, Tech. rep., 1984.

Ladstätter-Weißenmayer, A., Heland, J., Kormann, R., von Kuhlmann, R., Lawrence, M. G., Meyer-Arnek, J., Richter, A., Wittrock, F., Ziereis, H., and Burrows, J. P.: Transport and build-up of tropospheric trace gases during the MINOS campaign: comparision of GOME, in situ aircraft measurements and MATCH-MPIC-data, Atmos. Chem. Phys., 3, 1887–1902, doi:10.5194/acp-3-1887-2003, 2003.

Lee, H., Irie, H., Kim, Y. J., Noh, Y., Lee, C., Kim, Y., and Chun, K. J.: Retrieval of Aerosol Extinction in the Lower Troposphere Based on UV MAX-DOAS Measurements, Aerosol Sci. Technol., 43, 502–509, 2009.

Levelt, P. F., den Oord, G. H. J. V., Dobber, M. R., Malkki, A., Visser, H., de Vries, J., Stammes, P., Lundell, J. O. V., and Saari, H.: The Ozone Monitoring Instrument, IEEE T. Geosci. Remote, 44, 1093–1101, 2006.

Levy, R. C., Remer, L. A., and Dubovik, O.: Global aerosol optical properties and application to Moderate Resolution Imaging Spectroradiometer aerosol retrieval over land, J. Geophys. Res.-Atmos., 112, D13210, doi:10.1029/2006JD007815, 2007.

Li, X., Brauers, T., Shao, M., Garland, R. M., Wagner, T., Deutschmann, T., and Wahner, A.: MAX-DOAS measurements in southern China: retrieval of aerosol extinctions and validation using ground-based in-situ data, Atmos. Chem. Phys., 10, 2079–2089, doi:10.5194/acp-10-2079-2010, 2010.

Lyons, W. A. and Cole, H. S.: Fumigation and Plume Trapping on the Shores of Lake Michigan During Stable Onshore Flow, J. Appl. Meteorol., 12, 494–510, 1973.

Martin, R. V., Chance, K., Jacob, D. J., Kurosu, T. P., Spurr, R. J. D., Bucsela, E., Gleason, J. F., Palmer, P. I., Bey, I., Fiore, A. M., Li, Q., Yantosca, R. M., and Koelemeijer, R. B. A.: An improved retrieval of tropospheric nitrogen dioxide from GOME, J. Geophys. Res., 107, 4437, doi:10.1029/2001JD001027, 2002.

Martin, R. V., Jacob, D. J., Chance, K., Kurosu, T. P., Palmer, P. I., and Evans, M. J.: Global inventory of nitrogen oxide emissions constrained by space-based observations of NO_2 columns,

J. Geophys. Res., 108, 4537, doi:10.1029/2003JD003453, 2003.

Martin, R. V., Sioris, C. E., Chance, K., Ryerson, T. B., Bertram, T. H., Wooldridge, P. J., Cohen, R. C., Neuman, J. A., Swanson, A., and Flocke, F. M.: Evaluation of space-based constraints on global nitrogen oxide emissions with regional aircraft measurements over and downwind of eastern North America, J. Geophys. Res., 111, D15308, doi:10.1029/2005JD006680, 2006.

McGuire, M. L., Jeong, C. H., Slowik, J. G., Chang, R. Y. W., Corbin, J. C., Lu, G., Mihele, C., Rehbein, P. J. G., Sills, D. M. L., Abbatt, J. P. D., Brook, J. R., and Evans, G. J. Elucidating determinants of aerosol composition through particle-type-based receptor modeling, Atmos. Chem. Phys., 11, 8133–8155, doi:10.5194/acp-11-8133-2011, 2011.

McLaren, R., Salmon, R. A., Liggio, J., Hayden, K. L., Anlauf, K. G., and Leaitch, W. R.: Nighttime chemistry at a rural site in the Lower Fraser Valley, Atmos. Environ., 43, 5847–5852, 2004.

McLaren, R., Wojtal, P., Majonis, D., McCourt, J., Halla, J. D., and Brook, J.: NO_3 radical measurements in a polluted marine environment: links to ozone formation, Atmos. Chem. Phys., 10, 4187–4206, doi:10.5194/acp-10-4187-2010, 2010.

MOE: Ministry of the Environment, Ontario (MOE): Air Quality in Ontario 2005 Report and Appendix, available online at: http://www.ene.gov.on.ca/environment/en/resources/STD01_076445.html, last access: 25 November 2011, 2011.

Müller, J. F.: Geographical-Distribution and Seasonal-Variation of Surface Emissions and Deposition Velocities of Atmospheric Trace Gases, J. Geophys. Res.-Atmos., 97, 3787–3804, 1992.

NASA: NASA Goddard Space Flight Center LAADS Web – Level 1 and Atmosphere Archive and Distribution System, available online at: http://ladsweb.nascom.nasa.gov/, last access: 25 November 2011, 2010a.

NASA: NASA Goddard Space Flight Center Aura Validation Data Center, available online at: http://avdc.gsfc.nasa.gov/, 25 November 2011, 2010b.

NASA: NASA Goddard Space Flight Center AERONET – Aerosol Robotic Network, available at: http://aeronet.gsfc.nasa.gov/, last access: 25 November 2011, 2010c.

Pelletier, B., Santer, R., and Vidot, J.: Retrieving of particulate matter from optical measurements: A semiparametric approach, J. Geophys. Res.-Atmos., 112, D06208, doi:10.1029/2005JD006737, 2007.

Perliski, L. M. and Solomon, S.: On the Evaluation of Air-Mass Factors for Atmospheric Near-Ultraviolet and Visible Absorption-Spectroscopy, J. Geophys. Res.-Atmos., 98, 10363–10374, 1993.

Plane, J. M. C. and Smith, N.: Atmospheric Monitoring By Differential Optical Absorption Spectroscopy, vol. 24 of Spectroscopy in Environmental Science, John Wiley & Sons, Inc., West Sussex, UK, Chapter 5, p. 223, 1995.

Platt, U.: Differential Optical Absorption Spectroscopy (DOAS), vol. 127 of Air Monitoring by Spectroscopic Technique, Chemical Analysis Series, John Wiley & Sons, Inc., Hoboken, NJ, USA, p. 27, 1994.

Platt, U. and Perner, D.: Direct Measurements of Atmospheric CH_2O, HNO_2, O_3, NO_2, and SO_2 by Differential Optical Absorption in the Near UV, J. Geophys. Res., 85, 7453–7458, 1980.

Platt, U. and Stutz, J.: Differential Optical Absorption Spectroscopy: Principles and Applications, Springer, Berlin, Heidelberg, Germany, 2008.

Reid, N. W., Niki, H., Hastie, D., Shepson, P., Roussel, P., Melo, O., Mackay, G., Drummond, J., Schiff, H., Poissant, L., and Moroz, W.: The southern Ontario oxidant study (SONTOS): Overview and case studies for 1992, Atmos. Environ., 30, 2125–2132, 1996.

Schaap, M., Apituley, A., Timmermans, R. M. A., Koelemeijer, R. B. A., and de Leeuw, G.: Exploring the relation between aerosol optical depth and $PM_{2.5}$ at Cabauw, the Netherlands, Atmos. Chem. Phys., 9, 909–925, doi:10.5194/acp-9-909-2009, 2009.

Sills, D. M. L., Brook, J. R., Levy, I., Makar, P. A., Zhang, J., and Taylor, P. A.: Lake breezes in the southern Great Lakes region and their influence during BAQS-Met 2007, Atmos. Chem. Phys., 11, 7955–7973, doi:10.5194/acp-11-7955-2011, 2011.

Sinreich, R., Friess, U., Wagner, T., and Platt, U.: Multi axis differential optical absorption spectroscopy (MAX-DOAS) of gas and aerosol distributions, Faraday Discuss., 130, 153–164, 2005.

Solomon, S., Schmeltekopf, A. L., and Sanders, R. W.: On the Interpretation of Zenith Sky Absorption Measurements, J. Geophys. Res., 92, 8311–8319, 1987.

Strawbridge, K. B., and Synder, B. J.: Planetary boundary layer height determination during Pacific 2001 using the advantage of a scanning lidar instrument, Atmos. Environ., 38, 5861–5871, 2004.

Torres, O., Bhartia, P. K., Herman, J. R., Ahmad, Z., and Gleason, J.: Derivation of aerosol properties from satellite measurements of backscattered ultraviolet radiation: Theoretical basis, J. Geophys. Res.-Atmos., 103, 17099–17110, 1998.

UWYO: University of Wyoming (UWYO), College of Engineering, Department of Atmospheric Science Atmospheric Soundings, available online at: http://weather.uwyo.edu/upperair/sounding.html, last access: 25 November 2011, 2010.

Vandaele, A. C., Hermans, C., Simon, P. C., Carleer, M., Colin, R., Fally, S., Merienne, M. F., Jenouvrier, A., and Coquart, B.: Measurements of the NO_2 absorption cross-section from 42 000 cm^{-1} to 10 000 cm^{-1} (238–1000 nm) at 220 K and 294 K, J. Quant. Spectrosc. Ra., 59, 171–184, 1998.

Wagner, T., von Friedeburg, C., Wenig, M., Otten, C., and Platt, U.: UV-visible observations of atmospheric O_4 absorptions using direct moonlight and zenith-scattered sunlight for clear-sky and cloudy sky conditions, J. Geophys. Res.-Atmos., 107, 4424, doi:10.1029/2001JD001026, 2002.

Wagner, T., Dix, B., von Friedeburg, C., Friess, U., Sanghavi, S., Sinreich, R., and Platt, U.: MAX-DOAS O_4 measurements: A new technique to derive information on atmospheric aerosols – Principles and information content, J. Geophys. Res.-Atmos., 109, D22205, doi:10.1029/2004JD004904, 2004.

Wagner, T., Burrows, J. P., Deutschmann, T., Dix, B., von Friedeburg, C., Frieß, U., Hendrick, F., Heue, K.-P., Irie, H., Iwabuchi, H., Kanaya, Y., Keller, J., McLinden, C. A., Oetjen, H., Palazzi, E., Petritoli, A., Platt, U., Postylyakov, O., Pukite, J., Richter, A., van Roozendael, M., Rozanov, A., Rozanov, V., Sinreich, R., Sanghavi, S., and Wittrock, F.: Comparison of box-air-mass-factors and radiances for Multiple-Axis Differential Optical Absorption Spectroscopy (MAX-DOAS) geometries calculated from different UV/visible radiative transfer models, Atmos. Chem. Phys., 7, 1809–1833, doi:10.5194/acp-7-1809-2007, 2007.

Wagner, T., Deutschmann, T., and Platt, U.: Determination of aerosol properties from MAX-DOAS observations of the Ring

effect, Atmos. Meas. Tech., 2, 495–512, doi:10.5194/amt-2-495-2009, 2009.

Wagner, T., Beirle, S., Brauers, T., Deutschmann, T., Frieß, U., Hak, C., Halla, J.D., Heue, K. P., Junkermann, W., Li, X., Platt, U., and Pundt-Gruber, I.: Inversion of tropospheric profiles of aerosol extinction and HCHO and NO_2 concentrations from MAX-DOAS observations in Milano in summer 2003 and comparison with independent data sets, Atmos. Meas. Tech. Discuss., 4, 3891–3964, doi:10.5194/amtd-4-3891-2011, 2011.

Wang, J. and Christopher, S. A.: Intercomparison between satellite-derived aerosol optical thickness and $PM_{2.5}$ mass: Implications for air quality studies, Geophys. Res. Lett., 30, 2095, doi:10.1029/2003GL018174, 2003.

Wenig, M. O., Cede, A. M., Bucsela, E. J., Celarier, E. A., Boersma, K. F., Veefkind, J. P., Brinksma, E. J., Gleason, J. F., and Herman, J. R.: Validation of OMI tropospheric NO_2 column densities using direct-Sun mode Brewer measurements at NASA Goddard Space Flight Center, J. Geophys. Res.-Atmos., 113, D16S45, doi:10.1029/2007JD008988, 2008.

Wittrock, F., Oetjen, H., Richter, A., Fietkau, S., Medeke, T., Rozanov, A., and Burrows, J. P.: MAX-DOAS measurements of atmospheric trace gases in Ny-Ålesund – Radiative transfer studies and their application, Atmos. Chem. Phys., 4, 955–966, doi:10.5194/acp-4-955-2004, 2004.

Zieger, P., Weingartner, E., Henzing, J., Moerman, M., de Leeuw, G., Mikkilä, J., Ehn, M., Petäjä, T., Clémer, K., van Roozendael, M., Yilmaz, S., Frieß, U., Irie, H., Wagner, T., Shaiganfar, R., Beirle, S., Apituley, A., Wilson, K., and Baltensperger, U.: Comparison of ambient aerosol extinction coefficients obtained from in-situ, MAX-DOAS and LIDAR measurements at Cabauw, Atmos. Chem. Phys., 11, 2603–2624, doi:10.5194/acp-11-2603-2011, 2011.